

Galaxy walls in observed and simulated catalogues

A.G. Doroshkevich^{1,2}, R.Fong³, D.L. Tucker⁴, & V.Turchaninov²

¹*Theoretical Astrophysics Center, Juliane Maries Vej 30, DK-2100 Copenhagen Ø, Denmark*

²*Keldysh Institute of Applied Mathematics, Russian Academy of Sciences, 125047 Moscow, Russia*

³*Dept. of Physics, University of Durham, Durham, DH1 3LE, England*

⁴*Fermi National Accelerator Laboratory, MS 127, P.O. Box 500, Batavia, IL 60510, USA*

6 March 2003

ABSTRACT

In our theoretical papers we have used the Zel’dovich Approximation to provide a physical insight into the formation and evolution of large-scale structure in the Universe. Here, we demonstrate the correspondence between the physical quantities of the theory with observational measures obtained through statistical analyses that we have concurrently been developing. It provides the possibility of the direct physical interpretation of observations, to complement the more indirect, purely statistical approaches, such as correlation function and power spectrum analyses.

We have applied then our methods to the wall-like structure elements to be found in mock observational catalogues derived from N-body simulations, as well as to actual observational catalogues, the Las Campanas Redshift survey (LCRS) and Durham/UKST Redshift survey (DURS). The agreement of the estimates of our statistical parameters with the values expected from our theoretical calculations indeed shows them to be actual physical measures of the walls, such as their mean separation, sizes, galaxy surface density and internal velocity dispersion. The estimated parameters also provide, in particular, the present amplitude of perturbations, τ , which characterizes the present epoch of evolution reached by large-scale structure. Physically, the results show that walls are high density, partially relaxed, quasi-stationary objects.

The amplitude is, in turn, linked to the main parameters of the underlying cosmological models. We show that, for a Hubble constant, $H_0 \approx 65$ km/s/Mpc, the measures in low density models, such as the flat Λ CDM model with $\Omega_m \approx 0.3$ and the open CDM (OCDM) model with $\Omega_m \approx 0.5$, are, indeed, in good agreement with those of the observations. We show, further, that the measured wall characteristics are consistent with Gaussian initial perturbations and a CDM-like power spectrum. We roughly estimate then that the cosmological parameter, $\Gamma \approx \Omega_m h \approx 0.38 \pm 0.18$, and confirm the agreement of our results with the COBE measured amplitude for the initial perturbations.

Key words: cosmology: large-scale structure of the Universe — galaxies: clusters: general — theory.

1 INTRODUCTION

The existence of rich wall-like superclusters containing as large a fraction as $\sim(40\text{--}50)\%$ of the whole galaxy population is now well established through the investigations of both observed and simulated spatial galaxy catalogues. Due to their high overdensities above the mean density of galaxies, such superclusters can clearly be seen in the observed Las Campanas Redshift Survey (Shectman et al. 1996) and Durham/UKST Galaxy Redshift Survey (Ratcliffe et al. 1996), as well as in simulated catalogues of ‘galaxies’ (Cole et al. 1997, 1998; Jenkins et al. 1998) and dark matter (DM)

(Doroshkevich et al. 1999a, hereafter DMRT). Furthermore, these simulations confirm more analytical calculations that the formation of larger wall-like superclusters occurs due to a nonlinear anisotropic matter compression on typical scales $\sim 20\text{--}30h^{-1}$ Mpc, about half the typical separation between walls. Further progress in the study of the observed large-scale distribution of galaxies will be made with the quarter million galaxy 2dF redshift survey (Colless 2001) and the million galaxy Sloan Digital Sky Survey (SDSS EDR, Stoughton et al. 2002).

The possible identification of superclusters of galaxies with Zel’dovich pancakes were discussed by Thompson &

Gregory (1978) and Oort (1983). More recently, Demiański & Doroshkevich (1999, hereafter DD99) confirmed such a connection with the comparison of the statistical characteristics of walls in N-body simulations with the expectations of an approximate analytical model based on Zel'dovich's non-linear theory of gravitational instability (Zel'dovich 1970, 1978; Shandarin & Zel'dovich 1989). This approach connects the characteristics of structure with the main parameters of the underlying cosmological scenario and the initial power spectrum and allows one to estimate some of these parameters using the measured characteristics of walls. Using N-body simulations of DM distributions, it was found that for sufficiently representative samples of walls the estimates of the wall parameters could be made with a reasonable precision of better than 20% (DD99; DMRT; Demiański et al. 1999, hereafter DDMT).

In this paper we apply these methods, as discussed in DD99 and DDMT, to more realistic mock catalogues, that is, catalogues from N-body simulations which include not only the biased selection of galaxies from the DM distribution, but also the observational selection functions of actual galaxy redshift surveys. This allows as direct as possible the comparison of the results from applying the same methods to the available observational catalogues, the Las Campanas Redshift Survey (LCRS), the Durham/UKST Galaxy Redshift Survey (DURS) and the SDSS. The LCRS and DURS have already been studied with various other analyses, resulting in estimates of the main characteristics of the large-scale distribution of galaxies (see, e.g., Landy et al. 1996; Ratcliffe et al. 1996, 1998; Doroshkevich et al. 1996, hereafter LCRS1; Tucker et al. 1997; Jing et al. 1998; Shandarin & Yess 1998; Doroshkevich et al. 1999b, hereafter LCRS2; Doroshkevich et al. 2000, Doroshkevich et al. 2002, hereafter LCRS3). In a further paper, Doroshkevich, Tucker & Allam (2002) also present some properties of the galaxy distribution in the SDSS EDR.

Although the approach provides then important statistical characteristics of the large-scale matter distribution, it is complemented by other methods, such as those proposed in Lee & Shandarin (1998); Schmalzing et al. (1999); Kercher (2000); Monaco & Efsthathiou (1999), which give a more complex description of large scale structure in the universe.

We now briefly introduce in Sec. 2 the theoretical ideas. In Sec. 3, we consider the methods of measurement and the corrections we need to apply for these characteristics of the matter distribution; a more detailed discussion can be found in previous papers. The results obtained for the simulated catalogues and the observed redshift surveys can be found in Secs. 4 and 5, respectively. We conclude with Sec. 6, where a summary and a short discussion of the main results are presented.

2 STATISTICAL CHARACTERISTICS OF LARGE-SCALE GALAXY DISTRIBUTION

In this section we briefly introduce the main characteristics of walls as described through a direct application of the Zel'dovich Approximation. Throughout this paper, a Harrison-Zel'dovich primordial power spectrum is assumed. For such a primordial power spectrum, the theoretical rela-

tionships were obtained in DD99 and were investigated in a corresponding DM simulation by DDMT.

2.1 Basic characteristics of perturbations

Thus, for a Harrison-Zel'dovich primordial power spectrum, the initial power spectrum is given as

$$p_{cdm}(k) = A(z)kT^2(k/k_0), \quad k_0 = \Gamma h \text{ Mpc}^{-1}, \quad (2.1)$$

$$\Gamma = \sqrt{\frac{1.7\rho_\gamma}{\rho_{rel}}} \Omega_m h.$$

Here k is the comoving wave number, $A(z)$ is the amplitude of perturbations at redshift z as described by linear theory, $T(x)$ is the CDM transfer function as given by Bardeen et al. (1986, hereafter BBKS), ρ_{rel} & ρ_γ are, respectively, the total energy density of relativistic particles, i.e., photons, neutrinos etc., and that due only to the photons, which today constitute the CMB.

In Zel'dovich's theory the basic physical characteristics of the large-scale matter distribution are suitably expressed through just two parameters: the coherence length of the initial velocity field, l_0 , and the variance of the random particles' displacement, σ_s^2 . The latter is also closely linked to the variance of the particle velocity. They have their simplest forms for the CDM-like power spectrum (2.1):

$$l_0^{-2} \equiv \int_0^\infty kT^2(k/k_0)dk = m_{-2}k_0^2$$

$$l_0 \approx 6.6 \Gamma^{-1} \sqrt{\frac{0.023}{m_{-2}}} h^{-1} \text{ Mpc}, \quad (2.2a)$$

$$\sigma_s^2 \equiv \frac{1}{2\pi^2} \int_0^\infty p_{cdm}(k)dk = \frac{A(z)}{2\pi^2} k_0^2 m_{-2} = \frac{A(z)}{2\pi^2 l_0^2}.$$

Together with the dispersion of the random particles' displacement, σ_s , we also use the dimensionless amplitude of perturbation,

$$\tau(z) \equiv \frac{\sigma_s(z)}{\sqrt{3}l_0} = \sqrt{\frac{A(z)}{6\pi^2}} l_0^{-2}. \quad (2.2b)$$

These parameters are closely linked to the variances of the (relative) density, σ_ρ^2 ,

$$\sigma_\rho^2 \equiv \left(\frac{\delta\rho}{\langle\rho\rangle} \right)^2 \equiv \frac{1}{2\pi^2} \int_0^\infty k^2 p_{cdm}(k)dk = \frac{A(z)}{2\pi^2} m_0 k_0^4.$$

$$\sigma_s^2 = \frac{\sigma_\rho^2}{m_0} \frac{m_{-2}}{k_0^2}, \quad \tau = \frac{m_{-2}}{\sqrt{3}m_0} \sigma_\rho(z)$$

Here (and further) we also make use of the spectral moments (BBKS), with the main moments being m_{-2} & m_0 :

$$m_{-2} \equiv \int_0^\infty xT^2(x)dx \approx 0.023, \quad (2.3)$$

$$m_0 \equiv \int_0^{k_{max}} x^3 T^2(x)dx \propto \ln^3(k_{max}/k_0)$$

The relations (2.1 & 2.2) demonstrate the close link of the characteristic scale, l_0 , and the dimensionless amplitude

of perturbation, τ , with the variance of particle displacements, σ_s . As was discussed in DD99, this parameterization is eminently suitable for the description of structure formation and evolution.

Observationally, there are several ways now of estimating these measures, with their different underlying assumptions. Thus, not only can we then compare the different estimates of these basic physical parameters of large-scale structure, but any significant difference in them would be very revealing of the assumptions made and, thus, of the nature of the catalogue under investigation.

2.2 The amplitude of perturbations

The evolution of DM structure shows a strong degree of self-similarity (DD99, DDMT), at least over the epochs and scales for which the Zel'dovich approximation remains a good description of the process. Indeed, in terms of 'dimensionless distances', i.e. distances in units of the characteristic scale, l_0 , the statistical properties of the large-scale structure of the DM distribution is then simply characterized by a single parameter, the dimensionless amplitude of perturbation, τ , of equation (2.2b); in cosmological models with different Ω_m & h the same evolutionary stage is reached for the same τ . Thus, as such, it also plays the role of time in Zel'dovich's theory.

Clearly, of the two parameters we have just introduced, it is the important parameter for characterizing the formation and evolution of large-scale structure. Thus, for the CDM-like power spectrum (2.1) such characteristics of large-scale structure as σ_8 , the variance of the mass within a random sphere of radius $8h^{-1}$ Mpc, certain integrals of the two-point correlation function of the matter distribution, $\xi(r)$, the amplitude of the quadrupole component of the CMB anisotropy, T_Q , and other measures of large-scale structure are all expressible through this 'time'. Some of these measures, however, are quite complicated functions of Γ , such as the familiar σ_8 . Naturally, we shall be concerning ourselves here with those measures that, for a CDM-like power spectrum, can be fairly simply expressed in terms of this dimensionless 'time', τ .

However, in reality, non-linear evolution distorts the power spectrum (especially on small scales) and that in turn leads to differences in the estimates for τ using these various observational measures of large-scale structure. There may well be other factors that can also distort some of these estimates. An example is the possible large-scale bias between the spatial distributions of DM and galaxies. On the other hand, this implies that these different estimates of τ can then be used to investigate and to quantify these important influences on the formation and evolution of structure and on the form of the actual power spectrum in comparison with an idealized CDM-like power spectrum.

We now provide here and in the other following subsections a list of the different estimators of 'time' at $z = 0$ that we shall study in this paper.

(i) The most fundamental characteristic of the amplitude comes from the measured large scale fluctuations of the CMB temperature. Using the fits for the CMB anisotropy proposed by Bunn & White (1997) we obtain for an open

universe with $\Omega_\Lambda = 0$, and a flat universe with $\Omega_\Lambda = 1 - \Omega_m$

$$\tau_T \approx 0.34 \left(\frac{h}{0.65} \right)^2 \left(\frac{\Omega_m}{0.5} \right)^{1.8} \left(\frac{m-2}{0.023} \frac{T_Q}{20\mu K} \right), \quad (2.4)$$

$$\sigma_s = 12h^{-1} \text{Mpc} \left(\frac{h}{0.65} \right) \left(\frac{\Omega_m}{0.5} \right)^{0.8} \sqrt{\frac{m-2}{0.023}} \left(\frac{T_Q}{20\mu K} \right),$$

$$\tau_T \approx 0.27 \left(\frac{h}{0.65} \right)^2 \left(\frac{\Omega_m}{0.3} \right)^{1.2} \left(\frac{m-2}{0.023} \frac{T_Q}{20\mu K} \right), \quad (2.5)$$

$$\sigma_s = 15.4h^{-1} \text{Mpc} \left(\frac{h}{0.65} \right) \left(\frac{\Omega_m}{0.3} \right)^{0.2} \sqrt{\frac{m-2}{0.023}} \left(\frac{T_Q}{20\mu K} \right),$$

where τ_T denotes the amplitude, $\tau(0)$, as estimated using the measured CMB anisotropy.

Obviously, this estimate relates to extremely large scales, \sim the horizon. It depends on the spectral moment $m-2$, which is insensitive to the form of the power spectrum at small scales and, thus, is essentially unchanged up to the present epoch and even well beyond, as at these large scales the evolution is still in the linear regime. However, we should correct T_Q for the possible contribution of gravitational radiation, which can decrease T_Q and, hence, τ_T by up to a factor of 2.

(ii) Of course, the amplitude of perturbations, τ , is also directly related to the Fourier transform of the power spectrum, the two point correlation function, $\xi(r)$:

$$3l_0^2 \tau^2 \equiv \sigma_s^2 = \lim_{r \rightarrow \infty} \int_0^r dx \left(1 - \frac{x}{r} \right) x \xi(x). \quad (2.6)$$

However, here we shall estimate τ using the galaxy correlation function from the observational and mock 2dF catalogues. We distinguish this estimator by the symbol, τ_ξ . Observationally, the galaxy correlation function for $r \lesssim 20h^{-1}$ Mpc is approximately given by the power law

$$\xi(r) = (r_0/r)^\gamma, \quad (2.7)$$

giving

$$\tau_\xi^2 \approx \frac{1}{3l_0^2} \frac{r_\xi^{2-\gamma} r_0^\gamma}{(2-\gamma)(3-\gamma)}, \quad (2.8)$$

where r_ξ denotes its first zero-point, i.e., we make the approximation that $\xi(r)$ follows the power law, equation (2.7), for $r \leq r_\xi$ and is zero for $r > r_\xi$. Although r_ξ is not at all well known, with estimates $\sim 20\text{--}40h^{-1}$ Mpc, values in this range do not have a significant effect of the final estimate of τ_ξ , since for $\gamma \approx 1.5\text{--}1.8$, $1 - \gamma/2 \approx 0.25\text{--}0.10$. Because the actually measured distribution is used here, this estimator is more sensitive to scales $r \approx 5\text{--}20h^{-1}$ Mpc.

The nonlinear clustering of galaxies at $r \leq r_0$ increases the estimate (2.8) of τ_ξ , but this distortion is not very strong, since the integral (2.6) converges at $r \rightarrow 0$. A further important difference between this and the previous estimator is that τ_ξ is affected by the possible large-scale bias that may be expected between the DM and galaxy spatial distributions. Comparison of τ_ξ with other estimators (Sec. 4.6.3) shows that the measure (2.6) usually underestimates the amplitude.

(iii) DD99 showed that, in the regime in which the

Zel'dovich approximation is valid, the dispersion of the peculiar velocity of a mass particle,

$$\sigma_{vel}(z) = u_0 \sqrt{3}\tau, \quad (2.9)$$

with

$$u_0 = -l_0 H_0 \left(\frac{1+z}{\tau} \frac{d\tau}{dz} \right)_{z=0} = 660 \frac{\beta}{\Gamma} \text{ km/s}, \quad (2.10)$$

$$\beta \approx \frac{2.3\Omega_m}{1 + 1.3\Omega_m},$$

Thus, we can use the measured velocity dispersion, σ_{vel} , to obtain another estimator of the ‘time’,

$$\tau_{vel} \equiv \frac{\sigma_{vel}}{\sqrt{3}u_0}. \quad (2.11)$$

Because σ_{vel} integrates also high velocities generated by the gravitational compression of matter (in particular, within clusters of galaxies), τ_{vel} actually estimates an upper limit for the amplitude of perturbations.

2.3 Statistical characteristics of walls in real space

In this Section we introduce five physical characteristics of structure that can be derived in the Zel'dovich Approximation (DD99). They are the particle surface density of walls, m_w , the wall separation and thickness, D_{sep} & h_w , the velocity dispersion of the particles within walls, w_w , and the dispersion of the velocities of the walls themselves, σ_v . As they can also be found ‘directly’ from the point distributions of N-body simulations, simulations have thus been used to confirm that the theoretical expressions so derived do indeed correspond to the actual physical quantities (DDMT). Our interest here is to understand how the quantities may be affected by the imposition of a realistic observational selection function, as in the mock 2dF catalogues, and, in particular, how some of them may then be observationally determined.

2.3.1 Surface density of walls

The most well-defined physical property of walls is their surface density, m_w , the number of galaxies per unit area. The approximate expression for the probability distribution function (PDF) of m_w based on the Zel'dovich Approximation has been obtained in DD99 using a technique similar to the Press-Schechter formalism. For Gaussian initial perturbations with the CDM-like power spectrum it can be written as follows:

$$N_m \approx \frac{1}{\sqrt{2\pi}\tau} \frac{1}{\sqrt{q_w}} \exp\left(-\frac{q_w}{8\tau^2}\right) \text{erf}\left(\sqrt{\frac{q_w}{8\tau^2}}\right), \quad (2.12)$$

$$q_w = \frac{m_w}{l_0 \langle n_{gal} \rangle}, \quad \langle q_w \rangle = 8(0.5 + 1/\pi)\tau^2 \approx 6.55\tau^2,$$

where $\langle n_{gal} \rangle$ is the mean density of galaxies in the sample (see equation (2.2a) for l_0 and (2.2b) for τ). The expression (2.12) connects τ with the mean surface density of walls and it can be estimated from the measured $\langle q_w \rangle$ as

$$\tau_m \approx \sqrt{\frac{\langle q_w \rangle}{6.55}}, \quad (2.13)$$

i.e., τ_m is the estimate of the dimensionless ‘time’, τ , obtained from the measured mean surface density of walls, $\langle q_w \rangle$.

2.3.2 The wall separation

We have not yet a simple theoretical description of wall separation. Nonetheless, taking into account the mainly one dimensional character of wall formation, we can roughly link the mean measured wall separation, $\langle D_{sep} \rangle$, to the mean surface density of walls, $\langle q_w \rangle$.

Indeed, the matter conservation law along the direction of wall compression can be approximately written as follows:

$$\langle m_w \rangle \approx f_w \langle n_{gal} \rangle \langle D_{sep} \rangle, \quad \langle q_w \rangle \approx f_w \langle D_{sep} \rangle / l_0$$

where f_w is the matter fraction assigned to walls. It implies that on average a fraction f_w of the particles situated within $\pm 0.5 \langle D_{sep} \rangle$ from the center of a wall will be collected in the wall. Although not relevant for this paper, we simply note here that when the mean wall separation is comparable to the size of catalogue, D_{cat} , the more accurate relation

$$\langle q_w \rangle \approx \frac{f_{dq}}{l_0} \left\langle \frac{D_{sep}}{1 + D_{sep}/D_{cat}} \right\rangle. \quad (2.14)$$

needs to be used (DDMT). Here f_{dq} denotes the matter fraction assigned to walls as measured from Eq. (2.14). The averaging can be performed analytically assuming a Poissonian exponential distribution function for the separations between walls.

2.3.3 Wall velocities

The velocity of walls, v_w , is the most simple physical property of large-scale structure to interpret. Although walls are clearly non-linear structures, the wall velocity is not yet distorted by the effect of small-scale clustering and by the relaxation of compressed matter. For Gaussian initial perturbations, the PDF of wall velocities, $N(v_w)$, is also expected to be Gaussian. The mean velocity, $\langle v_w \rangle$, is expected to be negligible compared with its dispersion, σ_v , which is linked to the amplitude of initial perturbations as $\sigma_v \approx u_0 \tau$, (2.9) (DD99 and DDMT). The measured dispersion of wall velocities, σ_v , provides then another estimate of the dimensionless ‘time’, τ ,

$$\tau_v = \sigma_v / u_0. \quad (2.15)$$

2.3.4 Velocity dispersion of galaxies within walls

The expected expression for the velocity dispersion of galaxies accumulated by walls, w_{wz} , can also be found from the Zel'dovich Approximation. Using the technique described in DD99 and DDMT, we find

$$w_{wz}^2(q, \tau) \approx u_0^2 \left(\frac{q_w^2}{12} + \frac{\tau^2(\beta+1)^2 q_w}{3\beta^2} \right), \quad (2.16)$$

where β , u_0 & q_w were introduced by (2.11) & (2.12). This function, in fact, characterizes the mean kinetic energy of the particles accumulated within a wall of given size, q_w . After averaging over the N_m PDF, equation (2.12), we obtain for the expected mean kinetic energy of particles in walls,

$$w_z^2(\tau) = \langle w_{wz}^2 \rangle \approx u_0^2 \tau^4 \left(7.4 + \frac{2.2(\beta+1)^2}{\beta^2} \right). \quad (2.17)$$

2.3.5 Wall thickness

The methods discussed in DD99 and DDMT also allow us to obtain the thickness of walls along the direction of maximal compression, h_{wz} , as described by the Zel'dovich theory:

$$h_{wz}(q, \tau) \approx 2l_0\tau\sqrt{q_w}, \quad (2.18)$$

Here h_{wz} is normalized to the thickness of a homogeneous slice with the same surface density. After averaging over the PDF (2.12), we have for the mean thickness of walls

$$\langle h_{wz} \rangle \approx 8\pi^{-1/2}l_0\tau^2. \quad (2.19)$$

Thus, with the theoretically derived surface density of (2.12), we obtain the expected compression factor as

$$\delta_z = \left\langle \frac{q_w l_0}{h_{wz}} \right\rangle \approx \frac{\langle \sqrt{q_w} \rangle}{2\tau} \approx \frac{2}{\sqrt{\pi}} \quad (2.20)$$

and δ_z is independent of redshift. The small value of the mean overdensity (2.20) is a natural result of using the Zel'dovich Approximation, as it does not describe the relaxation of compressed matter during the strongly non-linear formation of gravitationally bound walls.

2.3.6 Properties of relaxed matter

As was shown in DDMT, in N-body simulations the dark matter compressed within walls is partly relaxed, and the walls are gravitationally bound. As usual, the relaxation results in the evaporation of higher energy particles and in the redistribution of the bound particles across a wall. The relaxation is essentially accelerated by the strongly inhomogeneous matter distribution within walls and, in particular, by the formation of high density clouds.

The relaxation partially destroys correlations of equations (2.16) & (2.18) between the surface density of wall, q_w , the velocity dispersion, w_{wz} , and wall thickness, h_{wz} , and makes the wall characteristics more random. Nonetheless, these characteristics remain correlated.

Analysis of the properties of simulated DM walls (DDMT) showed that after relaxation the wall thickness, h_w , and the velocity dispersion within walls, w_w , are linked to the surface density of walls, q_w , as follows:

$$w_w = \langle w_w \rangle \mu^{p_w} \omega, \quad h_w = \langle h_w \rangle \mu^{p_h} \zeta, \quad (2.21)$$

$$\mu = m_w / \langle m_w \rangle = q_w / \langle q_w \rangle$$

where the factors μ^{p_w} & μ^{p_h} describe the regular variations of w_w & h_w with the surface density of walls, with the *reduced* velocity dispersion, ω , and *reduced* wall thickness, ζ , characterizing the random variations of these quantities. For the DM walls in N-body simulations, DDMT found that

$$p_w \approx p_h \approx 0.45 - 0.55, \quad \langle w_w \rangle \approx w_z \sqrt{\epsilon}.$$

w_z was introduced in equation (2.17). Now, $\epsilon = \langle w_w^2 \rangle / w_z^2 \sim 0.2 - 0.5$ characterizes the lost of kinetic energy as compared with the expectations of Zel'dovich's theory and, so, also represents the degree of relaxation reached by the walls. The PDFs of the reduced velocity dispersion and thickness, N_ω and N_ζ , are also found to be roughly fitted by Gaussian functions with

$$\langle \omega \rangle \approx \langle \zeta \rangle \approx 1, \quad \sigma_\omega \approx 0.3 - 0.4, \quad \sigma_\zeta \approx 0.5 - 0.7, \quad (2.22)$$

2.4 Wall properties in redshift space

With the observations, we generally only have redshifts for the galaxies and not their actual radial positions. This will distort some of the parameters we have just introduced in Sec. 2.3. However, from their analyses of N-body simulations, DDMT found that q_w is still connected with the amplitude, τ_m , by the same relations (2.12) & (2.13), but as might be expected, the wall thickness is distorted by the 'finger of God' effect.

Thus, in redshift space, it is the velocity dispersion within walls that would characterize the observed effective thicknesses of walls along a line of sight. In Zel'dovich's theory, the velocity dispersion is identical to (2.16). The thickness, normalized as before (see Sec. 2.3.5),

$$h_{wz} = \sqrt{12} \frac{w_{wz}}{H_0} = l_0 [q_w^2 \beta^2 + 4\tau^2 q_w (\beta + 1)^2]^{1/2}, \quad (2.23)$$

As we will see in Sec. 4 it is larger than the real space thickness by $\sim 1.5 - 2$ times.

For actual observational catalogues the transversal and radial directions are, thus, not equivalent and the measurements of wall parameters in these different directions provide independent characteristics of wall properties. In particular, the transversal size of walls are not essentially influenced by velocities and can then be considered as an unperturbed estimator of the wall thickness in real space.

3 MEASURED CHARACTERISTICS OF LARGE SCALE MATTER DISTRIBUTION.

3.1 Selection of structure elements

A sample of wall-like structure elements can be constructed from catalogues using the two parameter method of DMRT, LCRS2 and Doroshkevich et al. (2000). With this method wall-like structure elements are identified with clusters found for some appropriate threshold linking length, l_{thr} , and threshold richness, N_{thr} . For volume limited catalogues, the threshold linking length characterizes then the overdensity, δ_{thr} , above the mean density at the cluster boundary,

$$\delta_{thr} = b^{-3} = \frac{3}{4\pi \langle n_{gal} \rangle l_{thr}^3}, \quad (3.1)$$

where $\langle n_{gal} \rangle$ is the mean density of galaxies in the sample, with b so defined a dimensionless linking length. The threshold richness, N_{thr} , restricts the fraction of galaxies, f_{gal} , associated with walls.

However, for catalogues constrained by selection effects, we need to modify this procedure. In particular, for most magnitude limited redshift surveys, the observed galaxy density varies appreciably with distance and a corresponding variation of linking length with redshift should then be used. We discuss this in next Sec.

3.2 The Selection Function

For both the observed and simulated mock catalogues the density of galaxies varies with distance due to the galaxy selection function. As the selection function is known, its systematic effect can then be partly compensated for by introducing the corresponding correction. Here we shall provide a brief outline of the method.

For many catalogues the selection function, f_s , can be well fitted to the expression (Baugh & Efstathiou 1993)

$$dN_{gal}(r) = f_s dr \propto x^2 \exp(-x^{1.5}) dr, \quad x = r/R_{sel}, \quad (3.2)$$

where the typical scale R_{sel} depends on the particular catalogue. This means that the observed galaxy distribution becomes homogeneous if instead we use the artificial radial coordinate, $r_a(r)$, rather than the real radial coordinate, r , where

$$r_a^3 = \int_0^r f_s dr = 2R_{sel}^3(1 - (1+y)e^{-y}), \quad (3.3)$$

$$y = \left(\frac{r}{R_{sel}}\right)^{1.5}.$$

For $r \ll R_{sel}$, $y \ll 1$, and $r_a \approx r$.

Applying then the standard MST (minimal spanning tree) technique to the artificial catalogue allows us to produce a more adequate set of structure elements. The procedure improves significantly the estimates of some of the structure parameters, such as, for example, the mass function of structure elements. As we show below, the measured wall parameters are also found then to have only a weak dependence upon the depth of catalogue.

However, even this more complicated procedure cannot restore lost information and including the more distant region of the catalogue, where a very strong selection effect applies, does not increase significantly the total number of galaxies in the sample. Moreover, as only very bright galaxies can be seen in such distant regions, walls get broken up, which would introduce additional uncertainty in the sample of structure elements. Our practice shows that for rich catalogues it is best to restrict the analysis by some reasonable distance limit. Although it then decreases the statistics of walls, the results are found to be more reliable. Still, if these distant low density regions are specially interesting, they can, in any case, be investigated separately.

3.3 Core-sampling

The core-sampling approach was proposed in Buryak et al. (1994) for the analysis of the galaxy distributions within deep pencil beam redshift surveys. In its original form it allowed us to obtain the mean free-path between the filaments and walls separately. It was improved in LCRS1, where some characteristics of the galaxy distribution were found for the LCRS. Its simple form was used in DDMT to characterize properties of the wall-like component of structure for simulated dark matter distributions and mock catalogues.

In this simple form of core-sampling the galaxies of the sample are distributed in a set of radial conical cores with a given angular size θ_c or in a set of tubular cores oriented along arcs of right ascension with a size d_c . All galaxies are projected on the core axis and its 1D distribution along this axis investigated.

This method turns out to be very suitable for the description of wall properties, as it deals with a sample of galaxies disposed within relatively narrow cores that helps suppress the influence of the random shape of walls. It provides more stable estimates of the characteristics of walls as compared with the Inertia Tensor method used in LCRS2 and in Doroshkevich et al. (2000) for the LCRS and DURS.

The characteristics obtained with the core-sampling method are the same as those discussed in Sec. 2.

Two factors restrict the application of this method for deep surveys. Firstly, the linear size of radial core increases rapidly with distance and, for more distant regions, the overlapping of walls when projected to the core axis becomes significant. This overlapping distorts the measured wall parameters and, in fact, destroys the main idea of the core-sampling approach. On the other hand, the small linear size of the core at small distances does not provide the effective averaging of wall characteristics over the core. For such cores the small scale clustering of galaxies within walls distorts the results at small distances, increasing the random scatter in the measurements.

The same reasons dictate the choice of the size of the tubular cores oriented along arcs of right ascension. In this case, although the selection function is constant for any given core, it varies from core to core. Also, the length of the core depends on its distance. This means that the contribution of the closest (shorter) and furthest (empty) cores is small and, in fact, increases the random scatter of the measurements.

This discussion shows that, for deeper surveys, better results are obtained by dividing the survey into several subsamples over the distance and analysing each subsample independently. The criteria for selecting walls and for the sizes of the sampling cores can then be chosen appropriately depending on the distance of the subsample. Thus, such a division helps take into account more adequately the influence of the selection function and decreases the random scatter of the resulting estimates.

3.4 Measured characteristics of walls

In applying objectively core sampling to a sample of wall-like structures as selected using the techniques of Secs. 3.1 and 3.2, the catalogue is considered as any other catalogue of particles. Sampling cores are obtained from the catalogue and the particle positions projected to the core axis. Completely ignoring how the particles were selected in the first place, a 1-dim clustering analysis is performed on these projected positions, using a linking length l_{link} .

However, the random intersection of walls with the sampling cores always results in a number of artificial poor clusters. To suppress the influence of this factor and to obtain the characteristics of actual rich walls a threshold richness, N_{min} , for clusters is used. But for too large an N_{min} the number of selected clusters decreases and the statistical estimates can become unreliable. The choice of an optimal linking length, l_{link} , is also important, since for smaller l_{link} the high density parts of a wall are then separated out, whereas for larger l_{link} the overlapping of wall projections becomes more important.

The measured wall parameters are sensitive to the influence of small scale clustering of matter within walls. The action of this factor is partly suppressed for larger sizes of the sampling core, θ_c & d_c . However, as discussed in Sec. 3.3, the linear size of a radial core increases rapidly with distance and, for the more distant regions and larger size of core, the artificial overlapping of wall projections again becomes essential.

The influence of these factors cannot be entirely elim-

inated and, so, our final estimates are always distorted to some extent. The foregoing discussion indicates that we can keep these distortions to a minimum if we use core sampling parameters within some optimal range. Our results below, for both the observed and mock catalogues, are, thus, averaged over the optimal range of l_{ink} and θ_c & d_c . Still, as before, the estimates remain more sensitive to the parameters of wall selection, l_{thr} & N_{thr} , used to select the catalogue in the first place, prior to core sampling analysis. These factors, however, do not distort significantly the dispersion of wall velocities, σ_v , making this the best characteristic of evolutionary stage reached by the large-scale structure of the Universe.

3.4.1 Measurement and corrections of wall parameters

The velocity, v_{obs} , of a wall, the velocity dispersion, w_{obs} , of the galaxies within the wall, the position, r_w , and the proper size, h_{obs} , of the wall are found as follows:

$$v_{obs} = \frac{1}{N_m} \sum_{i=1}^{N_m} u_i, \quad w_{obs}^2 = \frac{1}{N_m - 1} \sum_{i=1}^{N_m} (u_i - v_{obs})^2, \quad (3.4)$$

$$r_w = \frac{1}{N_m} \sum_{i=1}^{N_m} r_i, \quad h_{obs}^2 = \frac{12}{N_m - 1} \sum_{i=1}^{N_m} (r_i - r_w)^2$$

where N_m ($\geq N_{min}$) is the number of particles in the cluster, i.e., wall, and r_i , u_i the coordinates and velocities of these particles along the sampling core. As before, the factor, 12, normalizes the wall thickness to that of a homogeneous slice with the same surface density of galaxies. The richness corrected for the selection effect, as discussed in Sec. 3.2, measures the surface density of the wall,

$$m_{obs} = \frac{N_m}{f_s(r_w) \theta_c^2 R_{sel}^2}. \quad (3.5)$$

As the measure of wall separation, D_{sep} , we simply take the distance between neighboring clusters.

These measures, m_{obs} , v_{obs} , w_{obs} and h_{obs} , are not identical to the parameters discussed in Sec. 2, as they measure quantities along the sampling core. They, thus, need to be corrected for the random orientation of the walls and sampling cores. The impact of this factor increases the measured surface density, as the corrected wall surface density,

$$m_c = m_{obs} \cos \phi, \quad 0 \leq \phi \leq \pi/2.$$

Thus,

$$\langle m_c \rangle = \int_0^{\pi/2} m_c \sin \phi d\phi = 0.5 \langle m_{obs} \rangle. \quad (3.6)$$

Here ϕ is the random angle between the core axis and the normal to the wall. For the wall velocity and thickness, the corrected values are

$$\langle v_c \rangle = \langle v_{obs} \rangle \sqrt{3}, \quad \langle h_c \rangle = \langle h_{obs} \rangle / \sqrt{3}. \quad (3.7)$$

For the velocity dispersion of galaxies within walls such a correction is not so important because the actual velocity dispersion is found to be almost isotropic (DMRT). In redshift space the corrected wall thickness is linked with the velocity dispersion as

$$\langle h_c \rangle = \sqrt{12} H_0^{-1} \sqrt{\langle w_w^2 \rangle}. \quad (3.8)$$

The measured PDF of wall surface densities, $N_m(m_{obs})$, is distorted due to small number statistics in the case of richer walls and the rejection of poorer walls with richnesses, $N_m \leq N_{min}$, as we've already discussed above. The same factors also distort the mean surface density of walls, $\langle m_c \rangle$. We, thus, correct the mean surface density by simply comparing the measured PDFs from the mock catalogues with the expected PDF, eq. (2.12).

To do this we will fit the measured PDF to the function

$$N_m = \frac{a_m}{\sqrt{x_m}} e^{-x_m} \text{erf}(\sqrt{x_m}), \quad x_m = \frac{b_m m_{obs}}{\langle m_{obs} \rangle}. \quad (3.9)$$

Here, b_m describes the deviations between the measured and expected mean surface densities of walls and a_w provides the normalization of the fit. So, if the measured PDF, $N_m(m_{obs})$, is well fitted to the function (3.9), then

$$m_t = \langle m_c \rangle / b_m \quad (3.10)$$

can be taken as the measure of the 'true' mean surface density of walls.

Finally, the measured mean dimensionless wall surface density, $\langle q_w \rangle$, and the amplitudes of perturbations, τ_m & τ_v , measured by the surface density and velocity of wall-like structure elements (2.13) and (2.15) can be found as follows:

$$\langle q_w \rangle = \frac{\langle m_{obs} \rangle F_s(D_{min}, D_{max})}{2b_m \langle n_{gal} \rangle},$$

$$\tau_m \approx \sqrt{\langle q_w \rangle / 6.55}, \quad \tau_v = \sqrt{\langle v_{obs}^2 \rangle} / u_0, \quad (3.11)$$

where u_0 and F_s have already been introduced with eqs. (2.11) and (3.4).

4 LARGE SCALE SIMULATED 'GALAXY' DISTRIBUTION

In an earlier paper, DDMT measured the above quantities for the DM catalogues of three N-body simulations, SCDM, OCDM and Λ CDM. They found that, for low density models, the resulting measures were indeed good estimates of the wall parameters and the corresponding theoretical quantities, establishing the potential of our methods of analyses for the investigation of large-scale structure. However, to relate our work with observations, we need now to apply our methods to more realistic simulated 'galaxy' catalogues, i.e., catalogues obtained from the N-body simulations using a realistic observational selection function. To this end, we make use of the publicly available mock galaxy redshift survey catalogues (Cole et al. 1998), which have been produced especially to simulate the very large 2dF survey of $\sim \frac{1}{4}$ million galaxies now being acquired at the Anglo-Australian Telescope. This will then allow us to investigate the impact on these measures of, in particular, the observational galaxy selection function and the spatial geometry of a realistic redshift survey, as well as the impact of the possible bias between galaxies and DM. We shall in the next Section even apply the methods to presently available galaxy redshift surveys to obtain preliminary estimates of the present evolutionary stage of large-scale structure in the Universe and, thus, of the cosmological mass density parameter, Γ .

We have here restricted ourselves to three mock 2dF catalogues from low Ω_m COBE normalized simulations.

Table 1. Parameters of mock catalogues

	Ω_m	h	N_{gal}	$\langle n_{gal} \rangle$	σ_8	τ_T	$\sigma_{vel}/\sqrt{3}$	τ_{vel}
O5-600	0.5	0.6	185477	0.006	0.9	0.29	471	0.31
L2-600	0.2	0.75	160332	0.006	0.9	0.22	336	0.21
L3-600	0.3	0.65	159067	0.006	1.05	0.27	451	0.27
L3-400	0.3	0.65	98780	0.01	1.05	0.27	418	0.25
slices	0.3	0.65	14711	0.007	1.05	0.27	384	0.23
DM	0.3	0.65	$7.08 \cdot 10^6$	0.06	1.05	0.27	471	0.28
gal	0.3	0.65	$2.10 \cdot 10^6$	0.17	1.05	0.27	471	0.28

Here τ_T , τ_{vel} and τ_v characterizes the amplitude as given by (2.5), (2.11) and (2.15).

4.1 Mock catalogues

Catalogues L2 & L3 are based on the flat Λ CDM model, with $\Omega_m = 0.2$ and 0.3 , respectively, whereas the catalogue O5 is based on the open CDM model having $\Omega_m = 0.5$. They are particularly attractive, since they promise large-scale structure similar to the observations, with L3 the presently generally favored model (see, e.g., Perlmutter et al. 1999; DMRT; Efsthathiou 1999). The catalogues, L2-600, L3-600, & O5-600, restricted to distances $100h^{-1}\text{Mpc} \leq D \leq 600h^{-1}\text{Mpc}$ allow us to investigate the sensitivity of our methods of analyses to different cosmological models when applied to catalogues having the realistic galaxy selection function and spatial geometry of an observational survey. To test the influence of the selection function itself the catalogue L3-400 with $100h^{-1}\text{Mpc} \leq D \leq 400h^{-1}\text{Mpc}$ (containing then $\sim 62\%$ of galaxies and $\sim 30\%$ of volume of the sample L3-600) was also studied. For a comparison with the LCRS, a mock LCRS catalogue of four slices with angular size $\delta = 1.5^\circ$ and magnitudes $18.5 \geq m \geq 16.15$ was also constructed from the L3-400 catalogue. For these slices the number of ‘galaxies’ and their selection function are similar to those in the LCRS. The basic characteristics of these five catalogues, L2-600, L3-600, O5-600, L3-400 & mock LCRS, are listed in Table 1, where N_{gal} is the number of ‘galaxies’, n_{gal} is the mean number density of the sample, σ_8 the amplitude of perturbations used and σ_{vel} the velocity dispersion of all the ‘galaxies’ in the catalogue. Finally, we need, of course, to also compare the results from the mock catalogues with those from the parent DM and ‘galaxy’ distributions in the full simulation cube. For this, we simply report on our analyses of the simulation based on the presently favoured cosmology, i.e., we present the results for the L3 simulation.

All mock catalogues reproduce the main observed characteristics of large-scale matter distribution (Cole et al. 1998; LCRS3). They have been prepared using the same random seed and differ only by the evolutionary degree reached for the present epoch. Correspondingly, the large-scale structures in all the models are similar to each other, whereas the degree of galaxy condensation and density contrast in the structures vary from simulation to simulation. For all catalogues the selection effect is well described by Eq. (3.2) with the characteristic scale $R_{sel} = 288 h^{-1} \text{Mpc}$. Thus, the region in which large-scale structure elements, walls in particular, are well sampled by these mock catalogues is that between $\sim 200\text{--}400 h^{-1} \text{Mpc}$.

Using equation (2.5), we can calculate τ_T , the value of the amplitude of perturbations, τ , expected at the present epoch for the large-scale structure in a COBE-normalized simulation. On the other hand, the observed growth of struc-

ture in the simulation is directly characterized by the actual velocity dispersion realized by the simulation. This measure is given by τ_{vel} , equation (2.11,) and, indeed, the two values are consistent with each other (Table 1) and the velocity dispersion, σ_{vel} , only weakly perturbed by the nonlinear processes at small scales.

4.2 General characteristics of simulated galaxy distribution

In the previous paper (LCRS3) some of the more general characteristics of the spatial galaxy distribution in the simulations and in the LCRS was discussed. LCRS3 constructed the Minimal Spanning Tree (MST) not only for each catalogue, but also for subsamples of richer wall-like structure elements. As expected, the galaxy selection function had a significant effect on some of the measures, but using the ‘modified’ catalogues to try to take into account the selection function did improve most of the measured characteristics of the galaxy distributions in these catalogues. They then found the general properties of the MSTs to be all similar, as were also the mass function and morphological distribution of structure elements.

In particular, the implication is that these catalogues can be taken as a reasonable basis for the investigation here of a more detailed quantitative comparison with the observed galaxy distribution.

4.3 Samples of selected walls

Samples of walls identified with richer clusters were selected in each of the four mock 2dF catalogues both in real and redshift spaces according to the procedure described in Sec. 3.2. They include $f_{gal} \approx 42\text{--}46\%$ of galaxies from the basic samples, which is consistent with the expected and observed fraction of galaxies in walls (DD99; LCRS1; LCRS2; DURS; LCRS3). As we noted in Sec. 4.1, the main fraction of galaxies in walls ($\sim 80\%$) is to be found between distances $200\text{--}400 h^{-1} \text{Mpc}$, where the observed richness of similar clusters varies by less than a factor of 2 due to the selection effect. Thus, the influence of the closer and more distant regions on the measures will be small.

In more detail, samples of walls were constructed for each of the catalogues, O5-600, L3-600 and L3-400, using two threshold linking lengths, $b_{thr}=1$ and $b_{thr}=0.8$. This was done not only in both real and redshift spaces, but also for the actual and modified catalogues, resulting in eight samples of walls for each of these three catalogues. To test the influence of farther regions of catalogues samples of walls

O5-400 were prepared from samples O5-600 by rejection of walls at the distances $D \geq 400h^{-1}\text{Mpc}$.

To study the influence of basic cosmological parameters two samples of walls, one from the actual catalogue and the other from the modified one, were constructed from L2-600 in both real and redshift spaces for the threshold linking length $b_{thr}=1$. To study the influence of the slice geometry two samples from the actual and modified catalogues were constructed from the mock LCRS catalogue of four slices in real space for the threshold linking length $b_{thr}=1$. However, to provide a more reliable comparison with the actual observed catalogue, the LCRS, six samples of walls from the actual and modified mock LCRS, with $b_{thr}=1.25$, $b_{thr}=1$ and $b_{thr}=0.8$, were constructed in redshift space.

To study the influence of the spatial geometry and the galaxy selection function of an actual redshift survey, one sample of DM walls and one of ‘galaxy’ walls with $b_{thr}=1$ was constructed using both the parent DM and ‘galaxy’ catalogues in real space from the full simulation cube, i.e., from L3.

Comparing the samples of walls constructed using L3-600 and O5-600, we find that the walls from the actual and modified catalogues have $\sim 65\text{--}75\%$ of common galaxies, whereas using L3-400 the fraction of common galaxies is increased to $80\text{--}85\%$. We expect then that the more robust estimates of the characteristics of spatial matter distribution will be obtained for the shallower samples, such as L3-400, and increasing the number of galaxies by using the deeper subsamples of the catalogue does not always improve the results, even though the more distant region contains $\sim 30\%$ of galaxies, but in $\sim 70\%$ of volume. The results listed in Table 2 illustrate these differences.

4.4 Statistical characteristics of simulated walls

LCRS3 made a study of the general character of walls. They found that the distributions of MST edge lengths characterised walls as sheet-like in redshift space. However, in real space the characterisation is found to be more complex, and the analysis begins to reveal walls as highly inhomogeneous. The two results quantitatively support a visual picture of walls as broken structures of closely knit filaments of ‘galaxies’, rich clumps and holes or voids. Here, we begin a more detailed analysis of walls and in this section we apply our core-sampling analysis of Secs. 3.3 and 3.4 and compare the results with the theoretical expectations given in Sec. 2.

4.4.1 Measurement and averaging

We then use core sampling analysis to estimate five basic characteristic measures of walls: the separation between walls, D_{sep} , wall thickness, h_w , dimensionless surface density, q_w , and the related overdensity in walls, δ , and the velocity dispersion of the ‘galaxies’ in walls, w_w . All these are, of course, average measures. Various estimates are made of them, using both radial conical and transverse cylindrical core samples. In redshift space the wall thickness, as measured along the radial direction, is mainly related to the velocity dispersion of the ‘galaxies’ within the wall, equation (3.8), which is readily seen from the comparison with the wall thickness measured in the transverse direction.

Two further characteristics were found using the real space catalogues only. Although walls are very large in size, they nonetheless also have their own proper or bulk motions. Clearly, the mean bulk motion will be zero and the interesting measure is the dispersion, σ_v , of the proper motions of the walls themselves along the axis of maximal compression. The other measure we estimate is the ratio, $\epsilon = w_w^2/w_z^2$, where w_z is the velocity dispersion predicted by the Zel’dovich Approximation for ‘galaxies’ in walls. It, thus, characterizes the degree of relaxation that the walls have reached at the present epoch (Sec. 2.4.5).

For radial conical cores, some care needs to be taken over the cone angle, θ_c , to use. With catalogue depths of $100h^{-1}\text{Mpc} \leq D \leq 600h^{-1}\text{Mpc}$, the growth of the cross-sectional size of the cone with distance leads at larger distances to walls being artificially merged when projected onto the axis of the cone. The effect is also worsened by the random shape that walls have. The result of these factors is the relatively strong variation of some of the measures with θ_c ; with the catalogues here we find the estimates for the wall thickness and velocity dispersion start to depend strongly on the cone angle for $\theta_c \geq 2.5^\circ$. At the other end of the scale for the cone angle, for $\theta_c \leq 1.5^\circ$, the small scale clustering of compressed matter begins to distort significantly the measured surface density in walls. Thus, $1.5^\circ \leq \theta_c \leq 2.5^\circ$ is the useful range of cone angles for the analysis of surveys of this depth. Nevertheless, we are partially helped by the fact that the analysis is dominated by the best observed walls being situated at moderate distances, $\sim 250 - 350h^{-1}\text{Mpc}$. The same factors restrict the choice of the size of the transversal cylindrical cores to the range, $6h^{-1}\text{Mpc} \leq d_c \leq 9h^{-1}\text{Mpc}$.

For O5-600, O5-400, L2-600, L3-600 and L3-400, the results were averaged over 9 cluster richness thresholds, $5 \leq N_{min} \leq 45$, over 5 linking lengths, $2h^{-1}\text{Mpc} \leq l_{link} \leq 4h^{-1}\text{Mpc}$, over 3 sizes of radial cone angles, $1.5^\circ \leq \theta_c \leq 2.5^\circ$, and over 4 sizes of transversal cores, $6h^{-1}\text{Mpc} \leq d_c \leq 9h^{-1}\text{Mpc}$, as well as over the samples of walls in the catalogue.

For slices the averaging was performed over 8 richnesses, $5 \leq N_{thr} \leq 26$, over 5 linking lengths, $2h^{-1}\text{Mpc} \leq R_{cls} \leq 4h^{-1}\text{Mpc}$, for a radial core size of $\theta_{core} = 1.5^\circ$, and for 4 sizes of transversal cores, $4h^{-1}\text{Mpc} \leq l_{core} \leq 7h^{-1}\text{Mpc}$.

Table 2 lists the results for real and redshift spaces separately. The scatter of an averaged wall parameter was taken as a measure of the error. The fact that most of the results are very similar for all the samples is an indication of the effectiveness of our analysis. In particular, they show how robust these measures are to the different geometries and selection effects in the different samples.

The probability distribution functions (PDFs) of the surface density of walls, N_m , of the wall velocity, N_v , and of the reduced wall thickness and velocity dispersion of ‘galaxies’ in walls, N_ω and N_ζ , are plotted in Fig. 1 for the L3-400 simulation. The dependence of the surface density of walls, q_w , with the linking length, l_{link} , are plotted in Fig. 2, for L3-600 and L3-400.

4.4.2 Basic characteristics of simulated walls

We now consider the significance of our results. We first notice the robustness of the measure, σ_v , for the dispersion of the bulk motions of walls, being quite insensitive

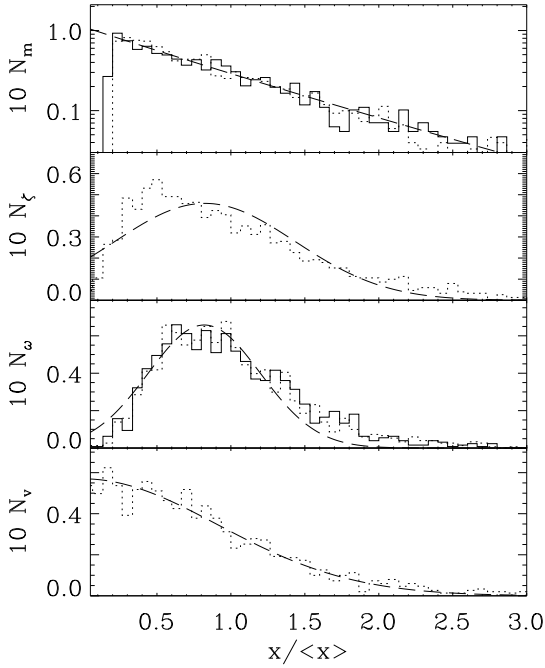


Figure 1. PDFs for the surface density of walls, $N_m(q_w/\langle q_w \rangle)$, the reduced wall thickness, $N_\zeta(\zeta_w/\langle \zeta_w \rangle)$, and reduced velocity dispersion, $N_\omega(\omega_w/\langle \omega_w \rangle)$, in real (dotted lines) and redshift (solid lines) spaces, and the PDF for the velocity of walls in real space, $N_v(v_w/\sigma_v)$, for the sample of walls in L3-400 mock catalogue.

to the different ways with which we made the measures. More importantly, it is gratifying that the amplitude, τ_v , we deduce from this estimate is so close to the corresponding expected amplitudes of the perturbations on large scales at the present epoch, namely, τ_{vel} and τ_T , as listed in Table 1. This corroborates the reasonableness of the N-body simulations, as it is really not at all clear that the procedures used for the simulations should produce the right degree of structure for the present epoch. Also, the PDF of this velocity, N_v , plotted in Fig. 1 for the L3-400 model, is well fitted to a Gaussian function, again in line with the theoretical expectations. Together with the estimate for τ_v , the agreement provides supporting evidence for Gaussian initial perturbations (DD99; DDMT).

In real space, the measured wall thicknesses are all very similar. However, the velocity dispersion of the ‘galaxies’ within walls increases the effective thickness of walls as observed in redshift space by about a factor of 2 in the radial direction, $\langle h_w^r \rangle$, compared to the real space measurements. Still, as expected, the redshift space measurement in the transversal direction, $\langle h_w^t \rangle$, is in agreement with those in real space. It is, of course, accompanied by a corresponding decrease of the wall overdensity, $\langle \delta^r \rangle$, as compared with those measured in the transversal directions, $\langle \delta^t \rangle$, and in real space.

The velocity dispersion of the ‘galaxies’ within walls, $\langle w_w \rangle$, is found to be about 1.5 times less than σ_{vel} , the velocity dispersion measured for the particles in the full simulation. Table 2 also shows that in real space $\langle w_w \rangle$ is weakly sensitive to the cosmological parameters, Ω and h , while in redshift space even such a weak dependence has disappeared, with $\langle w_w \rangle$ the same for all samples.

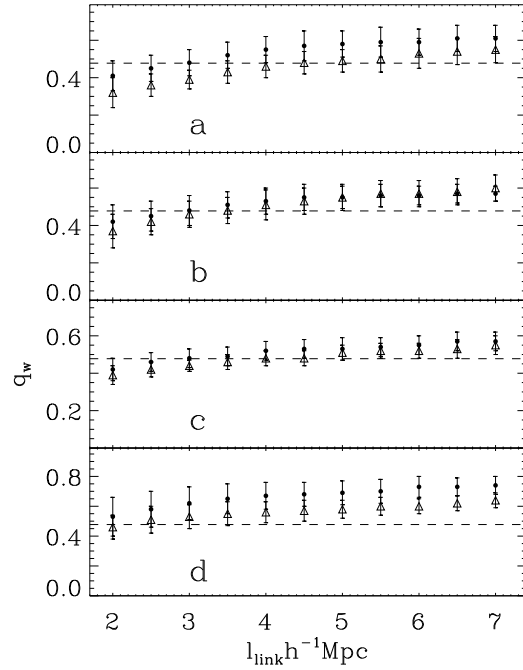


Figure 2. Functions q_w for $\theta_c = 1.5^\circ$ vs. the linking length, l_{link} , for two samples of wall-like structure elements (points & triangles) in L3-600 in real (panel a) and redshift (panel b) spaces and in L3-400, also in real (panel c) and redshift (panel d) spaces.

Both the dimensionless surface density of ‘galaxies’ in walls, q_w , and its related amplitude of perturbations at the present epoch, τ_m , are listed in Table 2. We also plot q_w as a function of linking length for both real and redshift space for the mock 2dF L3-600 and L3-400 catalogues. The figure shows how weakly dependent these measures are on linking length. Averaging of q_w and τ_m was performed over both radial and transversal cores. The small scatter, $\leq 20\%$, shows that they are also the same for both sets of cores. We also find that τ_m agrees with the expected amplitudes τ_{vel} and τ_T , as listed in Table 1, and, thus, also with the measured amplitude, τ_v . The PDFs of surface density, $N_m(q_w/\langle q_w \rangle)$, plotted in Fig. 1 for the L3-400 mock catalogue for both real and redshift space are well fitted to the theoretical expression, equation (2.16). Thus, this independent measure is also consistent with Gaussian initial perturbations.

The estimates for the mean wall separation are found to be similar in both real and redshift spaces; with such a large separation we cannot expect that the peculiar velocities of the ‘galaxies’ would affect the redshift space estimate. However, the wall separation measured along transversal cores is found to be larger by ~ 1.3 – 1.5 times than the measurement along radial cores. The difference can be attributed to the selection function, as it is absent for the complete parent samples in the rectangular simulation boxes and increases for the deeper ‘magnitude’ limited cone samples, O5-600 and L3-600, as compared with the shallower samples, O5-400 and L3-400. It demonstrates again the moderate efficacy of using the deeper catalogues. The effect is more important for smaller core sizes and larger threshold richnesses, due to the decrease in the number of richer walls, resulting in poorer statistics.

Table 2. Wall properties in mock catalogues

sample	$\langle q_w \rangle$	τ_m	τ_v	$\langle \delta^r \rangle$	$\langle \delta^t \rangle$ $h^{-1}\text{Mpc}$	$\langle h_w^r \rangle$ $h^{-1}\text{Mpc}$	$\langle h_w^t \rangle$ km/s	$\langle w_w \rangle$ $h^{-1}\text{Mpc}$	$\langle D_{sep}^r \rangle$ $h^{-1}\text{Mpc}$	$\langle D_{sep}^t \rangle$
real space										
O5-600	0.72 ± 0.14	0.33 ± 0.03	0.35 ± 0.05	3.4	5.2	6.0 ± 1.6	4.8 ± 1.1	351 ± 49	63 ± 10	79 ± 24
O5-400	0.72 ± 0.12	0.33 ± 0.03	0.31 ± 0.03	3.9	4.1	5.7 ± 1.5	5.0 ± 0.5	340 ± 24	58 ± 11	62 ± 13
L2-600	0.30 ± 0.08	0.21 ± 0.03	0.26 ± 0.02	3.1	5.0	5.0 ± 1.3	5.2 ± 1.4	247 ± 52	46 ± 18	74 ± 25
L3-600	0.44 ± 0.09	0.26 ± 0.03	0.32 ± 0.03	3.3	5.3	5.6 ± 1.5	4.9 ± 1.2	330 ± 67	50 ± 15	82 ± 25
L3-400	0.41 ± 0.07	0.25 ± 0.02	0.30 ± 0.01	4.3	4.6	4.8 ± 1.0	4.2 ± 1.0	305 ± 47	40 ± 8	63 ± 10
slices	0.45 ± 0.11	0.26 ± 0.03	0.31 ± 0.04	7.3	7.5	3.5 ± 0.7	3.1 ± 0.8	250 ± 38	35 ± 8	47 ± 12
DM	0.51 ± 0.07	0.28 ± 0.02	–	2.7	–	4.9 ± 0.5	–	245 ± 29	52 ± 5	–
gal	0.46 ± 0.06	0.26 ± 0.02	–	2.2	–	6.8 ± 1.5	–	354 ± 76	64 ± 12	–
redshift space										
O5-600	0.79 ± 0.17	0.34 ± 0.04	–	1.7	5.0	12.5 ± 2.6	4.5 ± 1.0	363 ± 77	63 ± 13	90 ± 20
O5-400	0.76 ± 0.15	0.34 ± 0.04	–	1.8	3.8	11.9 ± 1.8	5.5 ± 0.8	353 ± 80	55 ± 10	65 ± 15
L2-600	0.37 ± 0.09	0.23 ± 0.03	–	1.7	4.6	12.5 ± 3.1	6.1 ± 1.9	353 ± 75	53 ± 15	76 ± 25
L3-600	0.52 ± 0.11	0.28 ± 0.03	–	1.7	5.5	11.7 ± 3.5	5.5 ± 1.8	337 ± 88	55 ± 16	76 ± 21
L3-400	0.52 ± 0.09	0.28 ± 0.03	–	1.8	3.8	11.8 ± 2.1	6.5 ± 1.4	338 ± 65	43 ± 12	56 ± 8
slices	0.45 ± 0.12	0.26 ± 0.05	–	3.0	5.8	8.9 ± 1.8	3.8 ± 1.5	257 ± 53	48 ± 16	58 ± 11

4.4.3 Matter relaxation within walls

For all the real space samples, the ratio of the characteristic energy of compressed matter to that expected from the Zel'dovich theory is found to be $\langle \epsilon \rangle \sim 0.3\text{--}0.5$. Together with the large values for the overdensity in walls in real space and in the transversal directions in redshift space, $\langle \delta \rangle \sim 3\text{--}5$, this fact provides evidence in favour of the partial relaxation at the present epoch of the matter in walls. Further results supporting this conclusion are how the wall measures, $\langle w_w \rangle$, $\langle \delta \rangle$, $\langle h_w \rangle$, & $\langle \epsilon \rangle$, are all so weakly dependent on the cosmological model. For all the samples here, we have

$$w_w \approx \langle w_w \rangle \left(\frac{q_w}{\langle q_w \rangle} \right)^{p_w} \omega, \quad p_w \approx 0.55, \quad (4.1)$$

$$h_w \approx \langle h_w \rangle \left(\frac{q_w}{\langle q_w \rangle} \right)^{p_h} \zeta, \quad p_h \approx 0.5,$$

and the PDFs of the *reduced* velocity dispersion, N_ω , and *reduced* wall thickness, N_ζ , introduced by (2.21) and (4.1), are adequately fitted to Gaussian functions (as shown in Fig. 1 for the L3-400 model). In the analysis of DDMT, this partial relaxation is also seen in the simulated DM catalogues.

4.5 Walls in mock L3 and in the full simulation cube.

With the available mock catalogues, we are able to compare the results of our investigations of the wall properties with those for the actual DM distribution and ‘galaxy’ distributions in the simulation, from which the mock catalogues were obtained. For each distribution in the full simulation cube, a sample of wall-like elements with $f_{gal} \approx 0.44$ was then selected for analysis.

The more general characteristics of large-scale structure such as the shape of the PDF of MST edge lengths, the mass function and morphology of structure elements for these catalogues were discussed in LCRS3, and were found to be generally consistent with each other. Nonetheless, for clustering on small scales it was found that the DM in this simulation

is more strongly clustered than the ‘galaxies’. This stronger DM clustering is partly suppressed by the anti-bias procedure used in Cole et al (1998) for ‘galaxy’ selection.

The differences between the measured wall properties in the mock 2dF catalogues, L3-600 and L3-400, and those in the full ‘galaxy’ sample, L3, are found to be moderate. The larger variations of the results for δ , as compared with those of the mean wall surface densities, $\langle q_w \rangle$, and of the mean wall thickness, $\langle h_w \rangle$, are mainly a reflection of the correspondingly large variations in the mean number density for the various samples, n_{gal} listed in Table 1. It shows again how weakly dependent the measures are upon the galaxy selection function and the spatial geometry of the mock catalogues.

The velocity dispersion within DM walls was found to be less, ~ 1.5 times, than for the ‘galaxies’ in the full simulation cube and for the mock 2dF catalogues. Even so, these variations do not exceed the scatter. For the DM sample this velocity dispersion (as well as the wall thickness) increases with the size of the sampling core and with the linking length used, indicating its sensitivity to the stronger small scale inhomogeneities present in DM simulations due to the incorporation of high density clumps and filaments within the walls (small scale biasing). For the mock 2dF catalogues, L3-600 and L3-400, these inhomogeneities are already partially suppressed by the anti-biasing procedure used by Cole et al (1998) for selecting ‘galaxies’ and further suppressed by the action of the selection function.

4.5.1 Characteristics of walls in slices

The boundaries of the slice geometry of the LCRS will naturally cut through walls, giving rise to an artificial system of less massive irregular cloud-like structures. The analyses of the 2dF L3-400 and of the mock LCRS of four slices show how the slice geometry has affected the results. These slice results for the main wall measures, $\langle q_w \rangle$, $\langle \tau_m \rangle$, $\langle \tau_v \rangle$ and $\langle D_{sep} \rangle$, are listed in Table 2 and actually agree well with those found for the large area of sky L3-400 sample. Although the differences between the results for the other wall

characteristics listed in Table 2 are greater, they still do not exceed the errors in the measurements.

Larger differences are found for the velocity dispersions within walls, $\langle w_w \rangle$, and the wall thicknesses, $\langle h_w^r \rangle$, and $\langle h_w^t \rangle$, measured in redshift space. They are caused by the action of several factors, of which the main cause is the poorer statistical representativity of walls (~ 200 for the mock LCRS as against ~ 500 for the L3-400) and the more narrow range of admissible threshold parameters (see Secs. 4.3 and 4.5). Both factors can create a systematic shift of the measured characteristics, which is only partially compensated when we consider the larger sample with six slices (Sec. 4.3). It would seem then that even for a slice volume of $\sim 10^6 h^{-3} \text{Mpc}^3$, with some 30–40 walls in each slice, this is still not adequate for a fair sample of walls and some of the discussed characteristics are still only poorly estimated.

4.6 Amplitudes of perturbations

Some of the structure characteristics listed in Tables 1 & 2, such as τ_{vel} and τ_v , relate to the motion of ‘galaxies’ and are, consequently, sensitive to the distribution and motion of the DM component. Other characteristics, such as τ_m and q_m , relate directly to the ‘galaxy’ spatial distribution. Thus, a comparison of these characteristics allows us to make an estimate of the possible large scale bias between ‘galaxies’ and DM.

4.6.1 Amplitudes of perturbations and a possible large scale bias

The analysis performed in DDMT showed that a large-scale bias results in different estimates for the amplitude of perturbations, τ_m , based on the DM and ‘galaxy’ walls. Even if for the DM walls all the different estimates of the amplitude, namely, τ_{vel} , τ_v and τ_m , were very close to each other, it was found that for the mock ‘galaxy’ catalogues generated using the biasing scheme of DDMT $\tau_m > \tau_v \approx \tau_{vel}$, instead. However, the size of the difference depends upon the degree of bias.

For the mock catalogues here the biasing used by Cole et al. (1998) has a local character and is not similar to the large-scale bias discussed in DDMT. The comparison of amplitudes shows that such a *local* bias only weakly distorts the wall surface density and for all the samples of walls listed in Table 2 we indeed do have

$$\tau_{vel} \approx \tau_v \approx \tau_m^c \approx \tau_m^{rd}, \quad (4.2)$$

within the range of errors. Here τ_m^c & τ_m^{rd} denote the τ_m measured in real and redshift spaces, respectively. The ‘anti-bias’ between the DM and galaxy distributions results in a difference between τ_m and τ_v of only $\sim 10\%$, which is within the measurement errors.

4.6.2 Averaging of the amplitude

For the three cosmological models here the amplitudes depend mainly on the cosmological mass parameter, Γ . After averaging over the models we obtain

$$\langle \tau_{vel} / \sqrt{\Gamma} \rangle \approx 0.7 \pm 0.03, \quad \langle \tau_v / \sqrt{\Gamma} \rangle \approx 0.67 \pm 0.06,$$

$$\langle \tau_m^c / \sqrt{\Gamma} \rangle \approx 0.58 \pm 0.03, \quad \langle \tau_m^{rd} / \sqrt{\Gamma} \rangle \approx 0.61 \pm 0.03, \quad (4.3)$$

$$\langle q_m^c / \Gamma \rangle \approx \langle q_m^{rd} / \Gamma \rangle \approx 2.4 \pm 0.5,$$

$$\sigma_s = (7 \pm 0.7) \Gamma^{-1/2} \sqrt{\frac{m-2}{0.023}} h^{-1} \text{Mpc},$$

The scatter between these different ways of estimating τ does not exceed the errors in each of the estimates, confirming the relationships used between τ , q_m and Γ .

Eq. (4.3) shows that for these simulations, based on different cosmological models but with the same initial power spectrum and moderate amplitudes, $\tau \leq 0.3 - 0.4$, the dependence of the structure characteristics upon the cosmological parameters agrees well with the theoretical expectations (DD99). This fact, as well as the consistency seen in Fig. 1 of the distributions of the wall parameters in the simulations with the theoretical fits, corroborates the self similar character of the transformation of the initial velocity field to the large scale structure found using the Zel’dovich approximation.

4.6.3 Amplitude of perturbations and autocorrelation function

The amplitude of perturbations can also be estimated independently using the correlations function. For these simulations, Cole et al. (1998) showed that the correlation functions are consistent with that of the APM/Stromlo redshift survey (Loveday et al. 1995), which in redshift space is characterised by the parameters,

$$r_0 = (5.9 \pm 0.15) h^{-1} \text{Mpc}, \quad \gamma_\xi = 1.47 \pm 0.03. \quad (4.4)$$

$$r_\xi \approx (40 \pm 10) h^{-1} \text{Mpc}$$

Substituting in equation (2.8) we obtain

$$\sigma_s = (10.9 \pm 1.4) h^{-1} \text{Mpc}, \quad \tau_\xi = (0.95 \pm 0.12) \Gamma. \quad (4.5)$$

Comparing this with the estimates of τ_m , equations (4.3), would imply

$$\Gamma \approx 0.4 \pm 0.16. \quad (4.6)$$

This value is consistent with $\Gamma = 0.3$ for the O5-600 sample, but may be an overestimate for the L3-600 and L2-600 simulations, which have $\Gamma = 0.2$ & 0.15 , respectively, although for the present data they are only just outside the errors for this estimate, (4.6).

5 LARGE SCALE GALAXY DISTRIBUTION IN OBSERVATIONS

The general properties of the spatial galaxy distributions as observed in the LCRS and DURS were studied in LCRS-1, LCRS-2 and Doroshkevich et al. (2000). Here, we study the subsample of clusters that may be identified as ‘walls’.

5.1 Basic catalogues

5.1.1 LCRS, the Las Campanas Redshift Survey

The spatial geometry of the LCRS consists of six $80^\circ \times 1.5^\circ$ slices, with three in the North Galactic Cap – LCRS-1 ($\delta =$

-3°), LCRS-2 ($\delta = -6^\circ$), and LCRS-3 ($\delta = -12^\circ$) – and three in the South Galactic Cap – LCRS-4 ($\delta = -39^\circ$), LCRS-5 ($\delta = -42^\circ$), and LCRS-6 ($\delta = -45^\circ$). Each slice consists of a set of fields of angular size $1.5^\circ \times 1.5^\circ$. The precision of radial velocity measurements is estimated as 67 km/s (Shectman et al. 1996, where a detailed description of the LCRS can be found).

One part of the survey ($\approx 80\%$ of the galaxies) was acquired with 112 fibres in each field and includes galaxies with $15.0 < m_R \leq 17.7$, but the other part ($\approx 20\%$ of galaxies) used only 50 fibres in each field and restricted observations to galaxies with $16.0 < m_R \leq 17.3$. This needs to be taken into account in any study of the large-scale structure in the LCRS. Fortunately, slice 3 includes only 112-fibre fields and slice 2 is composed almost entirely of 50-fibre fields. For the other slices they are intermixed, causing then some additional disruption of the observed structures and decreasing the mean observed density of galaxies by about 20%.

Another peculiarity of the LCRS is the loss of close galaxy pairs due to the finite size of the fibres used (55 arc sec on the sky). This ‘fibre separation effect’ depresses the small scale clustering of galaxies and artificially reduces the measured richness of high density clumps. Using a fixed number of fibres will also tend to artificially homogenize fields of different richnesses, leading to some dilution of the richness of walls.

Of course, such artificial selection effects could distort our measured characteristics for walls in the LCRS. This means that the results obtained here for this catalogue have a *preliminary* character. However, our purpose here is simply to demonstrate the potential of the methods for the analysis of representative (and homogeneous) surveys, such as the forthcoming 2dF and Sloan surveys, when these wall characteristics can be measured with a fully quantitative assessment of the errors involved.

For this catalogue, the selection function (3.2) can be used with the dimensionless distance redefined as follows

$$x = r/R_{sel} - 0.44, \quad R_{sel} = 150h^{-1}\text{Mpc}. \quad (5.1)$$

The artificial catalogue with a uniform galactic density can also be constructed as described in Sec. 3.2. The best sampled part of the LCRS is situated at a distance of $D \approx 250h^{-1}\text{Mpc}$.

5.1.2 DURS, the Durham/UKST Redshift Survey

In the DURS redshifts were obtained for ~ 2500 galaxies in a $\sim 20^\circ \times 75^\circ$ area centered on the South Galactic Pole. They were selected through a random 1-in-3 sampling of galaxies with $b_J \leq 17$ mag in a complete galaxy catalogue, the Edinburgh/Durham Southern Galaxy Catalogue (Collins, Heydon-Dumbleton & MacGillivray 1989; Collins, Nichol & Lumsden 1992). The accuracy of the DURS radial velocity measurements is estimated to be 150 km/s. Further details of the survey and a brief account of the results of the analysis of DURS using more familiar techniques than here can be found in Ratcliffe et al. (1996, 1998).

For this catalogue the selection function (3.2) can be used with $R_{sel} = 88h^{-1}\text{Mpc}$ and the best sampled part of the DURS is situated at distances $D \approx 100\text{--}150h^{-1}\text{Mpc}$.

5.2 Wall properties in the LCRS and DURS

5.2.1 Selection of walls

To obtain reliable statistical results and also estimate the possible influence that our selection procedures have had on them, five samples of wall-like structure elements were selected in each slice of the LCRS for a depth of $D = 450h^{-1}\text{Mpc}$, using the modified catalogue (Secs. 3.1 & 3.2). For each slice, the selection was performed for $b_{thr} = 1$ (two sets of walls with $f_{gal} \approx 0.3 - 0.35$ and $f_{gal} \approx 0.4 - 0.45$), $b_{thr} = 1.13$ (one set of walls with $f_{gal} \approx 0.43 - 0.45$) and $b_{thr} = 1.25$ (two sets of walls with $f_{gal} \approx 0.4 - 0.43$ and $f_{gal} \approx 0.47 - 0.5$), so that the fraction of galaxies in walls is in the range, $0.4 \leq f_{gal} \leq 0.5$. Of each slice, one of the samples is, in fact, the same as that studied in LCRS2 and in LCRS3. For the DURS three sets of walls were selected in the same manner, but for a depth of $D = 350h^{-1}\text{Mpc}$.

The use of the modified catalogues enables us to account for the effect of the selection function, selecting wall-like structure elements through their overdensity. For the measured galaxy surface density in walls, we can also make the obvious correction for the observational selection effect. By practically eliminating the influence of the selection function, we find that the wall properties we study here become weakly sensitive to the depth of the catalogues. However, unavoidably, the scatter in the results are worsened by the artificial selections mentioned in Secs. 5.1.1 & 5.1.2 and by the impact of the small thickness of the LCRS slices.

5.2.2 Observed and simulated walls

A more detailed comparison of the walls selected from simulations and the observed LCRS using our MST analysis can be found in LCRS3. In particular, the comparison showed that all the samples of walls are similar with respect to their MST density distribution and morphology.

5.2.3 Basic characteristics of walls

Estimates for the mean wall parameters are listed in Table 3 for the LCRS and DURS catalogues restricted to the depths, $150h^{-1}\text{Mpc} \leq D \leq 350h^{-1}\text{Mpc}$ and $20h^{-1}\text{Mpc} \leq D \leq 350h^{-1}\text{Mpc}$, respectively. The optimal range of the linking lengths, core sizes and threshold richnesses used for averaging the results must combine reasonable representativity and the effective suppression of the random scatter in the final estimates (see discussion in Secs. 3.3, 3.4). Under these conditions, the averaging for the LCRS was done over 11 threshold richnesses, $5 \leq N_{thr} \leq 15$ and 11 linking lengths $2h^{-1}\text{Mpc} \leq l_{link} \leq 7h^{-1}\text{Mpc}$. The size of the radial cores was simply that of the LCRS slice thickness, $\theta_c = 1.5^\circ$, whilst for the cylindrical transversal cores we took 4 diameters in the range $4h^{-1}\text{Mpc} \leq d_c \leq 7h^{-1}\text{Mpc}$. For the DURS, averaging was performed over 9 threshold richness, $5 \leq N_{thr} \leq 13$ and 11 linking lengths $3.5h^{-1}\text{Mpc} \leq l_{link} \leq 8.5h^{-1}\text{Mpc}$. The DURS samples had a radial core size of $\theta_c = 5^\circ$ & 6° , and transversal core sizes of $d_c = 6$ & $7h^{-1}\text{Mpc}$. The errors are then taken as the rms scatter of the individual estimates, i.e., the 121 and 99 results from each threshold richness and linking length used for the LCRS and DURS, respectively. Part of the errors depends on the shape of the distribution

Table 3. Parameters of walls selected in the LCRS and DURS

sample	$\langle q_w/\Gamma \rangle$	$\tau_m/\sqrt{\Gamma}$	$\langle \delta^r \rangle$	$\langle \delta^t \rangle$	$\langle h_w^r \rangle$ $h^{-1}\text{Mpc}$	$\langle h_w^t \rangle$ $h^{-1}\text{Mpc}$	$\langle w_w \rangle$ km/s	$\langle D_{sep}^r \rangle$ $h^{-1}\text{Mpc}$	$\langle D_{sep}^t \rangle$ $h^{-1}\text{Mpc}$
LCRS-1	2.4 ± 0.7	0.60 ± 0.09	3.0	7.0	8.8 ± 1.7	2.9 ± 0.7	256 ± 49	56 ± 12	153 ± 28
LCRS-2	2.5 ± 0.9	0.61 ± 0.11	3.7	10.5	8.4 ± 1.8	2.6 ± 0.7	241 ± 48	59 ± 13	141 ± 26
LCRS-3	2.9 ± 0.9	0.66 ± 0.11	2.6	6.8	9.5 ± 1.7	3.1 ± 0.8	274 ± 52	52 ± 10	139 ± 24
LCRS-N	2.6 ± 0.9	0.63 ± 0.11	3.1	8.0	8.9 ± 1.7	2.8 ± 0.7	257 ± 50	55 ± 12	145 ± 26
LCRS-4	2.5 ± 0.8	0.61 ± 0.09	3.1	7.3	8.4 ± 1.8	2.8 ± 0.6	242 ± 52	68 ± 12	158 ± 29
LCRS-5	2.6 ± 0.9	0.63 ± 0.09	2.7	6.3	8.3 ± 1.4	3.1 ± 0.9	240 ± 48	60 ± 9	134 ± 28
LCRS-6	2.5 ± 0.8	0.62 ± 0.10	3.1	8.6	8.1 ± 1.5	2.5 ± 0.8	234 ± 38	64 ± 12	135 ± 25
LCRS-S	2.5 ± 0.8	0.62 ± 0.10	3.0	7.4	8.3 ± 1.5	2.8 ± 0.8	239 ± 46	63 ± 11	143 ± 28
$\langle LCRS \rangle$	2.5 ± 0.9	0.62 ± 0.10	3.0	7.7	8.6 ± 1.6	2.8 ± 0.7	247 ± 48	60 ± 9	147 ± 25
$\langle DURS \rangle$	2.2 ± 0.6	0.58 ± 0.08	1.7	6.5	9.7 ± 1.8	4.9 ± 1.2	280 ± 52	44 ± 10	35 ± 7

functions and, so, represents an ‘error on the method’. To obtain a more representative error on the measurement more samples will be required, although the close agreement, to better than 10%, between the estimates for $\langle q_w \rangle$ and τ_m from all six slices and, in particular, between the widely separated LCRS-N and LCRS-S is very encouraging for our approach. It is unfortunate that the DURS is both a little too shallow and a sparsely sampled survey to improve on the estimates, although it is again encouraging that the DURS estimates are in agreement with the LCRS results.

To test the impact of more distant low density regions the analysis was repeated for the set of walls selected for a maximum depth for the LCRS of $D_{max} = 450h^{-1}\text{Mpc}$. Although the results were found to be weakly sensitive to the maximum depth used, the scatter in the results did increase by $\sim 10 - 30\%$ for the deeper catalogue. On the other hand, the DURS is much more problematic as it is just a 1-in-3 randomly sampled catalogue, making it less ideally suited for such a detailed analysis of structure. However, although the results were less reliable than for the LCRS, the estimates did agree within the errors.

Eight parameters, namely, the dimensionless mean surface density of walls, $\langle q_w \Gamma^{-1} \rangle$, the measured amplitude of perturbations, $\langle \tau_m \Gamma^{-1/2} \rangle$, the mean overdensity above the mean density, $\langle \delta^r \rangle$ & $\langle \delta^t \rangle$, the mean wall thickness, $\langle h_w^r \rangle$ & $\langle h_w^t \rangle$, and separation, $\langle D_{sep}^r \rangle$ & $\langle D_{sep}^t \rangle$, along sets of radial and transversal cores were also obtained using the methods described in Sec. 3.5. The mean velocity dispersion of galaxies assigned to walls, $\langle w_w \rangle$, can, of course, only be found for the radial cores. The estimates of the main wall characteristics are found to have a relatively small scatter, $\sim 20\%$, and are similar for all six slices.

These observed wall parameters can be directly compared with those found from the N-body simulations, Sec. 4. The velocity dispersion of galaxies and the wall separation along radial cores are found to be similar in both simulated and observed catalogues. As was discussed in Secs. 2.4 & 3.4.1, the wall thickness measured along radial cores is identical to the velocity dispersion (Eq. 3.8). As shown by the simulations, the actual wall thickness is measured along transversal cores, since this is similar in both real and redshift spaces, Sec. 4.4.2.

The difference between wall thicknesses measured along radial and transversal cores, $\langle h_w^t \rangle \ll \langle h_w^r \rangle$, shows that, along a short axis, walls are gravitationally confined quasi-

stationary objects. Just as with the ‘Finger of God’ effect for galaxy clusters, the wall thickness along radial cores, as well as the measured velocity dispersion, characterizes the gravitational potential of compressed DM rather than the actual wall size.

For the DURS, as well as for all the large-area of sky simulated catalogues, the wall separation in both the radial and transversal directions are found to be similar. In contrast, for the slice survey of the LCRS a large difference, $\sim 2 - 2.5$ times, between the mean radial and transverse wall separations, $\langle D_{sep}^r \rangle$ & $\langle D_{sep}^t \rangle$, is found. A similar but less strong difference was also found for the simulated slices (Secs. 4.4.2 & 4.4.4). The differences may thus well be caused by the geometry of thin slices and amplified by the relatively small statistic of the richest walls. As was found in LCRS3, for small threshold richnesses, $N_{thr} \leq 5$, this difference disappears and the wall separations along transversal cores become closer to those along radial cores.

The wall parameters are found to be consistent with the estimates obtained in LCRS1, LCRS2 and Doroshkevich et al. (2000) using other different methods of analysis. In LCRS2, the mean wall thickness and the mean size of proto-walls were found to be $h_w \sim 5 - 6 h^{-1}\text{Mpc}$ and $R_{prw} \sim 20 - 23 h^{-1}\text{Mpc}$, similar to the values, $\langle h_w^r \rangle \sim (8.7 \pm 2) h^{-1}\text{Mpc}$ and $l_0 \langle q_w \rangle \sim (17 \pm 6) h^{-1}\text{Mpc}$, listed in Table 3. The mean wall separations, $\langle D_{sep}^r \rangle \approx (55 - 75) h^{-1}\text{Mpc}$, found for the LCRS2 sample having the depth, $D = 350 h^{-1}\text{Mpc}$, and $\langle D_{sep}^t \rangle \approx (50 - 70) h^{-1}\text{Mpc}$ for the similar LCRS1 sample are also similar to the estimates, $\langle D_{sep}^r \rangle = 60 \pm 9 h^{-1}\text{Mpc}$, listed in Table 3.

The mean velocity dispersions of galaxies, $\langle w_w \rangle = (247 \pm 48) \text{km/s}$, listed in Tables 3 for both LCRS and DURS is less than those compiled by Oort (1983a, b) of $300 - 350 \text{km/s}$ for the nearest superclusters of galaxies. It is also less than the pairwise galaxy velocity dispersion in the LCRS of $366 \pm 13 \text{km/s}$ (Szalay, Landy & Broadhurst 1998), and in the DURS of $387^{+96}_{-62} \text{km/s}$ (Ratcliffe et al. 1996). This difference demonstrates mainly the different physical nature of these dispersions.

5.2.4 Matter relaxation within walls

The strong correlation between the velocity dispersion within walls, w_w , and the surface density of walls, q_w , found in simulations (DDMT and Sec. 4) are also seen for the

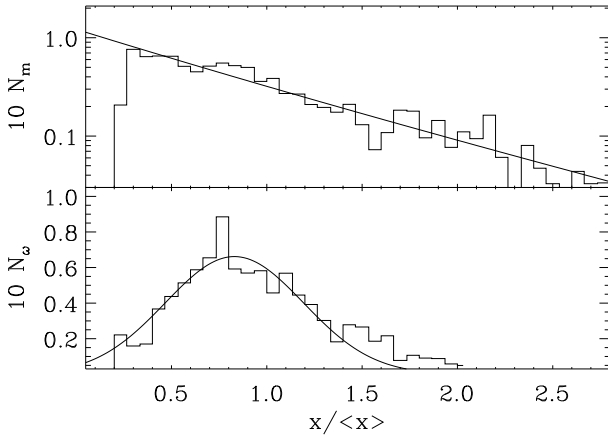


Figure 3. PDFs $N_m(q_w/\langle q_w \rangle)$, and $N_w(\omega/\langle \omega \rangle)$ averaged over one sample of walls selected in the LCRS for the same threshold parameters. Fits (2.12) and (2.22) are shown by solid line.

LCRS and DURS. For all the samples of walls in the LCRS the measured linear correlation coefficients of these parameters are ~ 0.4 – 0.5 , and the mass dependence of $w_w(q_w)$ is well described by (2.21) with $p_w \approx 0.5$. As discussed in DDMT the character of this correlation is also universal, supporting the prediction of the Zel'dovich Approximation for the strong correlation of w_w with q_w , equation (2.16). The PDFs plotted in Fig. 3 of the reduced velocity dispersion, N_w , can be roughly fitted by the expected Gaussian functions (see discussion in Sec. 2.3.6).

These results, together with the large difference discussed in the previous section for the wall thicknesses measured in the radial and transversal directions, argue in favor of the partial relaxation of matter compressed within walls and confirms that the walls are high density gravitationally confined and partially virialized (quasi-)stationary objects.

5.2.5 Dimensionless surface density of walls

The PDFs, $N_m(q_w)$ and $N_w(q_w)$, averaged over the set of walls selected using $b_{thr}=1.1$ in the five richer slices of the LCRS is plotted in Fig. 3. It shows that even with the relatively small statistic of walls in this sample the measured $N_m(q_w)$ is close to the theoretically expected distributions, (2.12) and (3.9). The result is then evidence in favour of the Gaussianity of initial perturbations, as the PDF (2.12) was derived for such a distribution of initial perturbations (DD99).

Plots of $\langle q_w \rangle$, as measured along radial cores, vs. l_{link} are shown in Figs. 4 & 5 for the three wall samples in the northern slices of the LCRS. For each l_{link} , measures were obtained for 11 threshold richness, $5 \leq N_{min} \leq 15$, and the average taken. The error bars shown are just the rms scatter of the measurements. The figures show the impact of the procedure of wall selection, slice richness and random intersections of walls and cores. It can then be seen that the measurements with smaller linking lengths, $l_{link} \leq 3.5 h^{-1} \text{ Mpc}$, pick out only the high density central parts of walls and, so, underestimate the actual surface density. For the poorer slices of the survey, LCRS-2 & LCRS-6, we find a larger scatter, while for other four slices the results are much more stable.

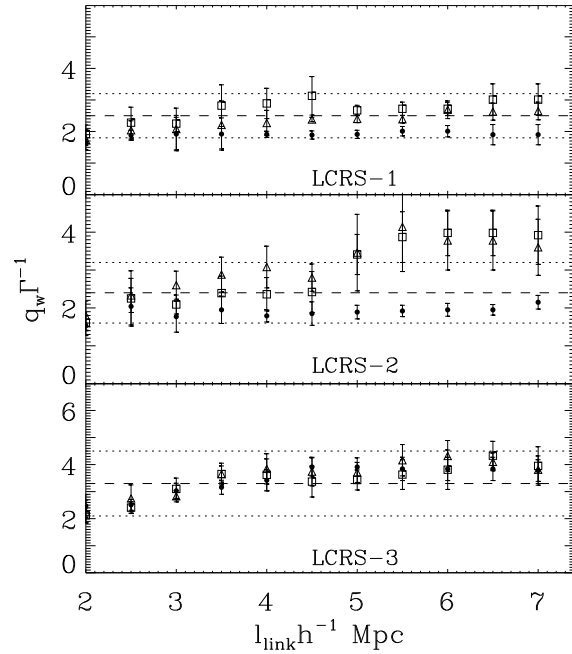


Figure 4. The dimensionless surface density, $q_w \Gamma^{-1}$, vs. the linking length, l_{link} , for three wall samples selected in northern slices of the LCRS for $b_{thr}=1$ (points), $b_{thr}=1.1$ (triangles) and $b_{thr}=1.25$ (squares). Mean values, $\langle q_w \rangle \Gamma^{-1}$, and scatter listed in Table 3 are shown by dashed and dotted lines.

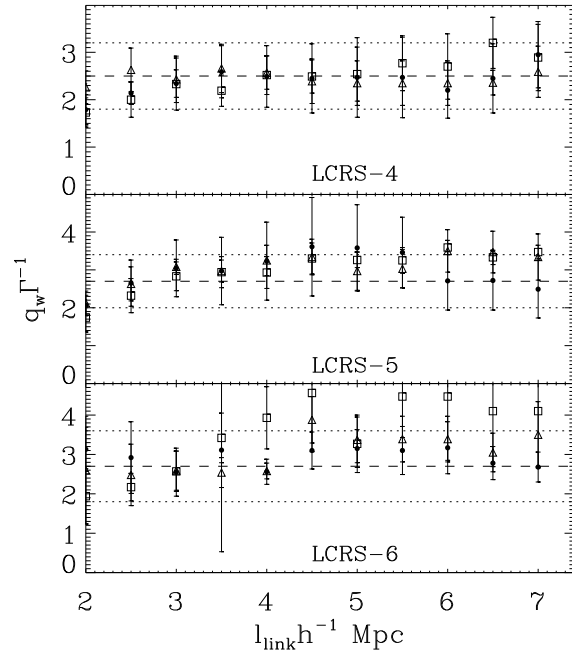


Figure 5. The dimensionless surface density, $q_w \Gamma^{-1}$, vs. the linking length, l_{link} , for three wall samples selected in southern slices of the LCRS for $b_{thr}=1$ (points), $b_{thr}=1.1$ (triangles) and $b_{thr}=1.25$ (squares). Mean values, $\langle q_w \rangle \Gamma^{-1}$, and scatter listed in Table 3 are shown by dashed and dotted lines.

For both the LCRS and DURS, Table 3 shows that the wall parameters,

$$\begin{aligned}\langle q_w \rangle &= (0.625 \pm 0.36)(\Gamma/0.25) \\ \tau_m &= (0.31 \pm 0.05) \sqrt{\frac{\Gamma}{0.25} \frac{m-2}{0.023}}, \\ \sigma_s &= (14.2 \pm 2.2) \sqrt{\frac{0.25}{\Gamma} \frac{m-2}{0.023}},\end{aligned}\quad (5.2)$$

agree well with those measured for the simulated catalogues (4.3). The uncertainties of $\sim 30\%$ for the measured dimensionless surface densities of walls are also similar to those listed in Table 2 for the four simulated slices. Unfortunately, for the LCRS, the varying field completeness (see Sec. 5.1.1) and the natural random variations in the wall samples cause significant slice-to-slice and sample-to-sample variations in the measured $\langle q_w \rangle$, restricting the precision of the estimates. A comparison with the results listed in Table 2 shows that with richer samples we can expect a precision $\sim 20\%$ or better.

For these parameters of the initial perturbations the expected velocity dispersion of galaxies is

$$\frac{\sigma_{vel}}{\sqrt{3}} \approx (440 \pm 60) \left(\frac{\beta}{0.5} \right) \sqrt{\frac{0.25}{\Gamma} \frac{m-2}{0.023}} \text{ km/s}, \quad (5.3)$$

with $\beta(\Omega_m)$ as defined in equation (2.11). Although, it is larger than the velocity dispersion, $\langle w_w \rangle$, within walls, as listed in Table 3, it is similar to that found in the simulations (Table 1). It will be interesting to see if this result holds with richer surveys such as the 2dF and Sloan.

5.2.6 Amplitude of perturbations as measured by the correlation function

The observed correlation functions of both the LCRS and DURS are well fitted by the standard power law (Jing et al. 1998; Ratcliffe et al. 1998):

$$r_0 = (5.06 \pm 0.12) h^{-1} \text{ Mpc}, \quad \gamma_\xi = 1.86 \pm 0.034, \quad (5.4)$$

$$r_0 = (6.8 \pm 0.3) h^{-1} \text{ Mpc}, \quad \gamma_\xi = 1.25 \pm 0.06, \quad (5.5)$$

for the LCRS and DURS, respectively. For both samples we can take the point at which the correlation function becomes zero as approximately

$$r_\xi \approx (40 \pm 10) h^{-1} \text{ Mpc}.$$

Using relation (2.8) we then have

$$\sigma_s = (14.6 \pm 2.1) h^{-1} \text{ Mpc}, \quad \tau_\xi = (1.3 \pm 0.18) \Gamma. \quad (5.6a)$$

$$\sigma_s = (9.8 \pm 2.6) h^{-1} \text{ Mpc}, \quad \tau_\xi = (0.86 \pm 0.23) \Gamma. \quad (5.6b)$$

for the LCRS and DURS, respectively. Comparison with (5.2) allows us to estimate for the LCRS, albeit with large uncertainty,

$$\Gamma \approx 0.24 \pm 0.14, \quad (5.7)$$

which agrees well with the similar estimate of (4.6), as well as with the estimate, $\Gamma = 0.2 \pm 0.03$, of Percival et al. (2001). As we saw in Sec. 4.5.4, the evaluation of wall properties

through the correlation function systematically underestimates the amplitude of large scale perturbations, σ_s , because the correlation function is only weakly sensitive to the perturbations on large scales, responsible for wall formation. Thus, the estimate (5.7) for Γ is in reality an upper limit rather than an actual value.

6 SUMMARY AND DISCUSSION

In this paper we continue the investigations of large-scale structure that we made in LCRS1, LCRS2, DMRT, DD99, DDMT, Doroshkevich et al. (2000) and LCRS3. The studies involved both observed redshift surveys and simulated catalogues from N-body simulations. The progress we made during these last few years in the interpretation of the measured statistical characteristics of wall-like structure elements allows us to repeat the analysis on large modern surveys, the LCRS and DURS, and to do a more detailed quantitative comparison of the measured characteristics of the observed large-scale galaxy distribution with those from modern simulations (Cole et al. 1998) and the predictions from Zel'dovich's theory of nonlinear gravitational instability (Zel'dovich 1970). Our analyses complements other approaches, such as that based on the percolation technique (Shandarin and Yess 1998) and the analysis of the 3D smoothed density field (Monaco & Efstathiou 1999).

An early result of Zel'dovich's theory was that the formation of sheet-like overdensities, the so-called Zel'dovich pancakes, is generic to the evolution of large-scale structure in the universe and early redshift surveys and galaxy supercluster catalogues (Thompson & Gregory 1978; Oort 1983) were already being interpreted in these terms. The observed walls are perhaps the most spectacular examples of Zel'dovich pancakes, appearing clearly as a result of non-linear evolution. Now we can compare the measured statistical characteristics of observed and simulated walls with the quantitative predictions of the theory for these measures. Of course, the Zel'dovich theory does not describe the relaxation of compressed matter and formation of gravitationally bounded quasi-stationary walls. But, we expect some of the characteristics are still closely connected to the weakly non-linear regime that is the domain of the Zel'dovich Approximation. Our comparisons confirm that some of these characteristics are indeed quite consistent with the theoretical expectations, thereby providing a physical insight into these aspects of the formation and evolution of large-scale structure in the Universe.

The surveys used are deep enough and well sampled enough to provide for the first time a fairly representative sample of wall-like structure elements and, thus, reasonable estimates of structure characteristics. At the same time, the significant scatter in the measurements of both observed and simulated walls shows that even with a volume as large as $\sim 10^6 h^{-3} \text{ Mpc}^3$ we still do not have a representative enough sample of walls and have yet to reach the statistically desirable stability for these estimates of wall characteristics. However, it is something we might have expected, as the 'effective depth' of these catalogues is only $200\text{--}300 h^{-1} \text{ Mpc}$ is itself comparable to the mean wall separation of $\sim 50\text{--}60 h^{-1} \text{ Mpc}$. Thus, the analysis will need to be repeated for more extended and larger catalogues. The results obtained

for the simulated catalogues, Table 2, show that for the complete 2dF survey the errors in the measurements for the main wall parameters can be improved by about a factor of 2. Our purpose here is to demonstrate the feasibility of our methods for obtaining useful measures of the characteristics of walls, of structures on scales of $\sim 50 h^{-1}$ Mpc.

6.1 Main characteristics of observed and simulated galaxy walls

6.1.1 Identification of walls

DDMT and LCRS3 showed from simulations that some 80% of the galaxies assigned to walls using the method described in Sec. 3 are the same both in the real and redshift spaces. The result confirms that the influence of the peculiar velocity of the galaxies does not perturb significantly the observed measures for the properties of walls, allowing then meaningful comparisons with the theoretical expectations based on the Zel'dovich Approximation. This also provides then independent estimates of cosmological parameter, Γ .

However, the range of the measured wall characteristics discussed in Sec. 4 (especially for slice surveys such as the LCRS) shows that the methods used for wall selection have sometimes difficulty in discriminating a high density wall from its environment. Usually, small variations in the measures caused by wall selection can be corrected for with the methods used. Nonetheless, such corrections are limited, and the analysis performed in Secs. 4 & 5 show that some of the characteristics of walls can be significantly perturbed.

In principle, two extreme situations are possible. Firstly, strong clustering criteria, as one might use, for example, in a search for Abell-like rich clusters, will result in a wall sample comprising only high density clumps and the central parts of walls. In opposite extreme case the selection results in a sample of artificially large walls, which include the extended halo and/or are formed due to the intermixture of projections of actually different walls. Nevertheless, the methods of wall identification described in Sec. 3.4 do allow the choice of optimal parameters and, thus, the avoidance of a strong over/under-estimation of wall richnesses.

6.1.2 Selection effect

Clearly, the galaxy selection functions of observed catalogues also pose a serious problem of wall identification. As was discussed in Sec. 3.2, the influence of the ordinary selection effect can be taken into account before wall identification. It, however, cannot restore lost information. Although it allows an increase of about only 20–30% in the size of the sample that one can analyse, it also generates a number of artificial walls, which appear mainly at large distances where the influence of the selection function is strongest. This ‘noise’ is aggravated by the increasing size with distance of the cross-section of radial sampling cores. This means that the smaller, but more reliable, wall samples can provide better results.

The simulations showed that for the sample L3-600 $\gtrsim 65\%$ of galaxies assigned to walls using the method of Sec. 3 are the same both with and without correction for the selection effect. This fraction of common galaxies increases to $\gtrsim 80\%$ for the less deep sample L-400. The test

confirms that increasing the number of galaxies in the sample for analysis does not always improve the robustness of the final result. Thus results listed in Table 2 for L3-600 and L3-400 are the same within the errors but, for the less deep catalogue the size of the errors are smaller. The same effect was found for the LCRS, for which the estimates of wall parameters obtained for the galaxy sample with distances, $150h^{-1}\text{Mpc} \leq D \leq 350h^{-1}\text{Mpc}$, had smaller errors than those obtained in the deeper sample, in which galaxies had distances $150h^{-1}\text{Mpc} \leq D \leq 450h^{-1}\text{Mpc}$ (see Sec. 5.2.3).

Still, the correction of wall samples for the selection function is found to be very useful in improving some of the measures, such as the important mass function of structure elements (LCRS3).

6.1.3 Measured characteristics of walls

The measured characteristics of walls are listed in Table 2 for the simulated catalogues in both real and redshift spaces and in Table 3 for the LCRS and DURS. With the simulations, it can be seen that the characteristic sizes and separation of walls are found to be only weakly sensitive to the basic cosmological model, if we restrict our considerations to low density models such as, for example, the Λ CDM and Λ CDM models.

The essential relaxation of matter within walls and accompanying effects is seen to strongly suppress the expected difference of wall parameters measured in real and redshift spaces and, in fact, most of the measured wall characteristics are found to be very similar in both spaces. The nature of the difference between the wall thickness along radial cores in these spaces is simply due to the ‘Finger of God’ effect, well known from the study of rich galaxy clusters. Indeed, as was shown in Secs. 2.4 and 3.4 (eq. 3.8), in redshift space the so-called wall thickness measures actually the velocity dispersion of compressed matter. The actual wall thickness is measured in redshift space along transversal cores, and, in the simulations, is naturally found to be the same as that measured in real space.

6.1.4 Surface density of walls

The surface density of walls, q_w , is the basic characteristic which is directly linked with the typical size of proto-walls (DMRT, LCRS2). The large values measured for the surface density is evidence in favour of the strong non-linear condensation of matter on unexpectedly large scales, which can reach $\sim 20 - 25h^{-1}\text{Mpc}$ for low density cosmological models. Such a large scale, comparable to the mean separation of walls of $\langle D_{sep} \rangle \approx 60h^{-1}\text{Mpc}$, agrees with the estimates of $f_{gal} \sim 0.40-0.45$ for the matter fraction accumulated in walls. This large fraction of galaxies assigned to walls demonstrates that walls must be considered not just as a very important structure element, but actually as forming the skeleton of the large-scale structure in the Universe.

The comparison of the wall surface densities in the three simulations here demonstrates that the differences in the surface density is caused by the factor, Γ , with the renormalized surface density, q_w/Γ , as well as all renormalized measures of amplitude, $\tau/\sqrt{\Gamma}$, the same (Sec. 4.6.2). It corroborates then the theoretical prediction of the self-similar

character of the evolution of the large-scale spatial matter distribution that DD99 found using the Zel'dovich Approximation.

The PDFs of both the observed and simulated surface densities of walls are found to be consistent with the theoretical fit, eq. 2.12, which was derived for Gaussian initial perturbations with the standard CDM-like power spectrum, supporting then the Gaussian nature of the initial perturbations.

However, the results obtained in Sec. 4 for the simulated 'galaxy' distribution show that even a sample of slices having as many as 4000–5000 galaxies in a volume of $\sim 10^6 h^{-3} \text{Mpc}^3$ is not representative enough, with differences for estimates of some of wall parameters as large as 30% between the slice catalogue and the full parent sample. This means that only with large redshift surveys such as the 2dF and SLOAN surveys can we hope to obtain representative quantitative estimates of the physical characteristics of large-scale matter distribution in the Universe. For such large catalogues, the precision of our estimates for the fundamental parameters, q_w/Γ and $\tau/\sqrt{\Gamma}$, can be improved, reaching a precision of $\sim 10\%$.

6.1.5 Relaxation of compressed matter

For a DM dominated universe the evolution of walls is defined by the behavior of the DM component and the galaxies can be considered as simply tracers of the evolution. The analysis of the simulated catalogues show that galaxies trace well the wall parameters and their peculiar velocities the essential relaxation of the matter compressed within walls. This relaxation is seen as a strong correlation between the velocity dispersion and the surface density of walls both in the real and redshift spaces, as a significant difference of wall thicknesses measured in the radial and transversal directions of redshift space and as a high overdensity exceeding that calculated using Zel'dovich's theory. The relaxation has then been significantly accelerated by the small scale clustering of compressed matter, taking it beyond the weakly non-linear regime of the Zel'dovich Approximation.

The PDFs of the reduced velocity dispersion, N_ω , are roughly fitted to Gaussian function parameters that are the same for all cases. For the observed catalogues, this statistic is still rather poor, even for the largest samples we studied, and the PDFs plotted in Figs. 3 for the LCRS are highly distorted.

These results show the walls to be high density, partially virialized, quasi-stationary objects, although at the present epoch they are beginning to be susceptible to break-up through the small scale disruption of compressed matter.

6.2 Amplitude and spectrum of perturbations

The amplitude and form of the power spectrum of density inhomogeneities in the Universe are the most fundamental characteristics of the perturbations. The problems of how these are related to the spatial distribution of matter have been widely discussed over the past twenty years, but until recently the situation has been far from clear. The estimates for the amplitude and spectrum obtained with different methods and for different observational samples differ in

many respects because the spatial distribution of different populations of objects is sensitive to different parts of the power spectrum and is, furthermore, differently biased due to the influence of physical, as well as observational selection, factors.

The analysis of the large-scale angular variations of the CMB continues to provide the most comprehensive determination of the initial power spectrum. The present data confirm that the large-scale part of the spectrum is well described by a power law with the spectral index, $n = 1 \pm 0.2$, consistent with the expected Harrison-Zel'dovich' power spectrum. The amplitude of these perturbations is then given by (2.4 & 2.5).

The results (5.2) give an estimate for the amplitude of perturbations for the LCRS and DURS as seen in the observed large-scale distribution of galaxies. Comparing these estimates, (2.4, 2.5 & 5.2), based as they are upon different observational data, provides now a reasonable estimate of the cosmological factor, Γ :

$$\Gamma \approx (0.32 \pm 0.04) \left(\frac{h}{0.65} \right)^{-0.15} \left(\frac{T_Q}{20\mu K} \right)^{-0.77}, \quad (6.1)$$

$$\Gamma \approx (0.21 \pm 0.05) \left(\frac{h}{0.65} \right)^{1.79} \left(\frac{T_Q}{20\mu K} \right)^{-1.43}, \quad (6.2)$$

for open CDM and flat Λ CDM models. These results are, indeed, consistent with the estimates of $\Omega_m \approx 0.3$, $\Omega_\Lambda \approx 0.7$, $\Gamma \approx 0.21$ from observations of high-redshift supernovae (Perlmutter et al. 1999), the values of the so-called 'concordance model' (see also discussion in Efstathiou 1999) and with the recent results from an analysis of the first section of the 2dF galaxy redshift survey (Percival et al. 2001)

$$\Gamma = 0.20 \pm 0.03. \quad (6.3)$$

An independent estimate of the spectral moment, σ_s , and amplitude of perturbations, τ_ξ , (4.5 & 5.7), were obtained from the galaxy correlation functions for APM, LCRS and DURS. This is not the same as finding the more well-known parameter, σ_8 , as they involve different combinations of r_0 , τ_ξ and γ_ξ . As we had discussed in Sec. 4.6.3, this approach probably overestimates the amplitude, τ_ξ & σ_s .

These results can also be considered as an independent corroboration of the COBE measurements of the CMB anisotropy, $T_Q \sim 20\mu K$, constraining then the possible contribution of gravitational radiation to the observed T_Q . The constraint is, however, model dependent, as our estimates of σ_s is affected by any possible large-scale bias between the spatial distributions of DM and galaxies and/or by a more complicated composition for the dark matter. These factors have been widely discussed over the past twenty years, but up to now their quantitative character is far from being well established. Indeed, the comparison of results such as these with those from other approaches will help to distinguish their influence and, with very large and more representative catalogues, we can begin to make quantitative estimates of their effect.

6.3 Large-scale bias between the spatial distribution of DM and galaxies and a possible composition of the DM component

The fact that the differences between our results for the characteristics of the simulated and observed large-scale matter distributions are small indicate that the simulations are providing a good description of the main features of the form and evolution of large-scale structure in the Universe. However, several factors that are still little understood may well prove significant, especially with the greater measurement precision that large observational catalogues promise. They are, among others, the possible large-scale bias between the spatial distributions of the DM component and galaxies and a more complicated composition of dark matter than in Λ CDM, such as, for example, in the MDM cosmological models.

A large-scale bias between the spatial distributions of the DM component and galaxies can be naturally generated during a reheating of the universe caused by the first objects to be formed (Dekel & Silk 1986 and Dekel & Rees 1987; more recently, Coles 1993, Sahni et al., 1994, Lee & Shandarin 1998, Demiański & Doroshkevich 1999, DD99, DMRT and LCRS2). DD99 calculated that such a bias could increase the concentration of galaxies inside richer walls by ~ 2 times.

Observationally, a large-scale bias certainly exists, as, for example, the difference in the relative concentration of baryons and luminous matter in galaxy clusters (e.g., White et al. 1993) and in the Böots void (Weistrop et al., 1992) would show. At the same time, the perfectly homogeneous distribution of Ly- α absorption systems seen in the spectra of quasars demonstrates a high degree of homogeneity in the spatial distributions of both the DM and baryonic components at high redshifts.

For the surveys we've studied here, the expected size of the bias is too small to be discernible, but, perhaps, for the much larger redshift surveys now being acquired, such a bias could give rise to a more significant difference between the amplitudes of perturbations measured by the galaxy correlation function and the wall surface density.

Acknowledgments

This paper was supported in part by Denmark's Grundforskningsfond through its support for an establishment of Theoretical Astrophysics Center. AGD also wishes to acknowledge support from the Center for Cosmo-Particle Physics "Cosmion" in the framework of the project "Cosmoparticle Physics". AGD would also like to acknowledge support under the Durham PPARC Visitors' Grant, as well as the PPARC STARLINK Project, as much of the analyses was made using the Durham STARLINK node.

REFERENCES

- Bahcall N.A., & Fan X., 1998, *ApJ*, 504, 1.
 Bardeen J.M., Bond J.R., Kaiser N., Szalay A., 1986, *ApJ*, 304, 15 (BBKS)
 Baugh C.M., & Efstathiou G., 1993, *MNRAS*, 265, 145.
 Bunn E.F., and White M., 1997, *ApJ*, 480, 6.
 Buryak O., Doroshkevich A., Fong R., 1994, *ApJ*, 434, 24.
 Cole S., Weinberg D.H., Frenk C.S., & Ratna B., 1997, *MNRAS*, 289, 37.
 Cole S., Hatton, S., Weinberg D.H. & Frenk C.S., 1998, *MNRAS*, 300, 945.
 Coles P., 1993, *MNRAS*, 262, 1065
 Colless M.M., 2001, *MNRAS*, 328, 1039
 Collins, C.A., Heydon-Dumbleton, N.H., MacGillivray, H.T., 1989, *MNRAS*, 236, 7P
 Collins, C.A., Nichol, R.C., Lumsden, S.L., 1992, *MNRAS*, 254, 295
 Dekel A. & Silk J., 1986, *ApJ*, 303, 39.
 Dekel A. & Rees M., 1987, *Nature*, 326, 455.
 Demiański M. & Doroshkevich A., 1999, *MNRAS*, 306, 779, (DD99).
 Demiański M., Doroshkevich A., Müller V., & Turchanin V.I., 2000, *MNRAS*, 318, 1177, (DDMT).
 Doroshkevich A., et al., 1996, *MNRAS*, 284, 1281, (LCRS1).
 Doroshkevich A.G., Müller V., Retzlaff J., & Turchanin V.I., 1999, *MNRAS*, 306, 575, (DMRT).
 Doroshkevich A. et al., 2000, *MNRAS*, 315, 767
 Doroshkevich A.G. et al., 2001a, *MNRAS*, 322, 369, (LCRS2)
 Doroshkevich A., Fong R., Tucker D.L., & Turchanin V.I., 2002, *MNRAS*, submitted. (LCRS3)
 Doroshkevich A., Tucker D., Allam S., 2002, *Proceedings of 5th RESCEU symposium "New Trends in Theoretical and Observational Cosmology"*, Universal Academy Press, in press
 Efstathiou G., 1999, *MNRAS*, 310, 842
 Jenkins A. et al., 1998, *ApJ*, 499, 20.
 Jing Y., Mo H., Boerner G., 1998, *ApJ*, 494, 1
 Kaiser N., 1984, *ApJ*, 284, L9
 Kercher M., 2000, *Lecture Notes in Physics*, 554, 36
 Landy S.D. et al., 1996, *ApJ*, 456, L1
 Lee J., & Shandarin S., 1998, *ApJ*, 500, 14.
 Loveday J., Maddox S.J., Efstathiou G., Peterson B.A., 1995, *ApJ*, 442, 457
 Monaco P, Efstathiou G., 1999, *MNRAS*, 308, 763
 Oort J.H., 1983a, *Ann.Rev.Astron.Astrophys.*, 21, 373
 Oort J.H., 1983b, *A&A*, 139, 211.
 Perlmutter S. et al., 1999, *ApJ*, 517, 565
 Percival W.J. et al., 2001, *MNRAS*, 327, 1297
 Ratcliffe, A. et al., 1996, *MNRAS*, 281, L47
 Ratcliffe A., Shanks T., Parker Q.A., and Fong R., 1998, *MNRAS*, 296, 73
 Sahni V., Sathyaprakash B.S., Shandarin S.F., 1994, *ApJ*, 431, 20.
 Schmalzing J., Gottlöber S., Klypin A., Kravtsov A., (1999), *MNRAS*, 309, 1007
 Shandarin S., Zel'dovich Ya.B., 1989, *Rev.Mod.Phys.*, 61, 185
 Shandarin S., Yess. C., 1998, *ApJ*, 505, 12.
 Shectman S.A. et al., 1996, *ApJ*, 470, 172.
 Stoughton S. et al. 2002, *AJ*, 123, 485; 576
 Szalay A.S., Landy S.D., Broadhurst T.J., 1998, in "Large Scale Structure: Tracks and Traces", ed. V.Müller, S.Gottlöber, J.Mücket, J.Wambsganss, World Scientific, p. 111
 Thompson L.A., Gregory S.A., 1978, *ApJ*, 220, 809.
 Tucker D.L. et al., 1997, *MNRAS*, 285, L5
 Weistrop D. et al. 1992, *ApJ*, 396, L23.
 White S.D.M., Briel U.G., & Henry J.P., 1993, *MNRAS*, 261, L8
 Zel'dovich Ya.B., 1970, *A&A*, 5, 20